N-type Organic Field Effect Transistor Based on Caffeine Derivatives

Cheng Zeng

A thesis

submitted in partial fulfillment of the

requirements for the degree of

Master of Science

University of Washington

2019

Committee:

Christine K. Luscombe, Chair

J. Devin MacKenzie

Program Authorized to Offer Degree:

Materials Science & Engr: Applied

University of Washington

Abstract

N-type Organic Field Effect Transistor Based on Caffeine Derivatives

Cheng Zeng

Chair of the Supervisory Committee:
Professor Christine K. Luscombe
Materials Science & Engineering

Field effect transistors, one of the most popular electronic devices, have drawn much attention due to their wide application in integrated circuits. Compared to the inorganic silicon-based FETs, organic field effect transistors (OFETs) have the advantage of being flexible and low-cost. As a result of this, OFETs have been extensively studied to improve their performance, including threshold voltage, on/off ratio and mobility. In this thesis, the first two chapters introduce semiconductor materials and devices. In Chapter 3, our work, the synthesis and fabrication of N-type OFETs is demonstrated. In our study, C-H activation, a cheap, green and environment-friendly method is used to make caffeine derivatives. Furthermore, two different alkyl substituents have been introduced to the caffeine unit to compare their performances in OFETs.

TABLE OF CONTENTS

LIST OF FIGURES

LIST OF TABLES

ACKNOWLEDGEMENTS

First, I would like to acknowledge Prof. Christine Luscombe, my academic advisor, for guidance and support, for giving project during my master's study. Also, I want to thank all the people in Luscombe Research Group, especially PhD student Yunping Huang for help on organic synthesis and PhD student Wesley Tatum for assistance on device fabrication. Besides, I'd like to express my thanks to Kristine Parra and Jiaxu Qin for help on characterization, Yongcao Zhang for advice and suggestions regarding devices.

Second, I'd like to appreciate my friends for encouragement, and without them, I cannot get through difficulties and successfully finish my master's study at University of Washington.

Last but not least, I express my deepest gratitude to my family, who sent me to study abroad, to expand my horizon, to know more about the world.

DEDICATION

I dedicate this thesis to my dearest parents.

Chapter 1. INTRODUCTION TO ORGANIC SEMICONDUCTORS

1.1 INTRODUCTION

As we come into the Information Age, the need for digital devices, including personal computers, mobile phones, tablets and flash drives, increases significantly. It is reported that in 2017, there were about 1 trillion unit shipments of semiconductor devices and silicon, being the most popular inorganic semiconductor, plays an important part in these devices due to its unique electrical properties and abundance on Earth.[1] However, the process to manufacture silicon semiconductors is complicated and expensive, including silicon purification, photolithography, etch, ion implant and more, which offsets the relatively cheap raw materials.[2] With the goal of making cheaper and better performance electronic devices, our focus has shifted to organic semiconductors. Organic semiconductors have the advantages of low-cost, flexibility and tunability, making them potential for next generation of electronics.

The development of organic semiconductors can be divided into three phases: organic crystals, small organic films and polymer films. The first one can date back to the early 20th century, when small organic anthracene crystal was discovered to have photoconductivity by Pope *et al.* in 1963, and later studied by Helfrich *et al.*.[3-5] Since then, molecular crystal semiconductors have attracted much attention, but the problem was that these kinds of devices required high voltages to operate, rendering it impractical to utilize in daily life.[6] For this reason, amorphous films from spin coating or vacuum deposition emerged to overcome this challenge. Although it didn't have the problem of high voltage, the performance was still not sufficient for commercial use. It was not until 1970s when doped conjugated polymer material, polyacetylene, was discovered by Heeger, MacDiarmid and Shirakawa, who were rewarded Nobel Prize in Chemistry

in 2000 that the field of organic semiconductor materials arose.[7] With increasing interest drawn to organic devices, a range of novel materials have been designed, such as perylene tetracarboxylic derivative and polythiophene, resulting in the rapid development of this field.[8, 9]

This chapter first discusses the structure of organic semiconductors and the underlying mechanism involved in conducting currents, then specific examples of organic semiconductors ranging from polymers to small organic chemicals are included. At last, a short conclusion is made, and the future of organic semiconductors is explored.

1.2 Structure of Organic Semiconductors

The structure of organic semiconductors is different from inorganic ones in terms of interactions occurring between molecules either or atoms. In inorganic semiconductors, such as silicon, atoms are covalently bonded to each other to form crystals, leading to strong interactions in neighboring atoms. On the other hand, organic counterparts are bonded to each other *via* π-interactions, a much weaker force compared to covalent bond, which implies distinctly different properties between the two. Electrical properties, like conductance, are typically the primary concern in the context of semiconductors.

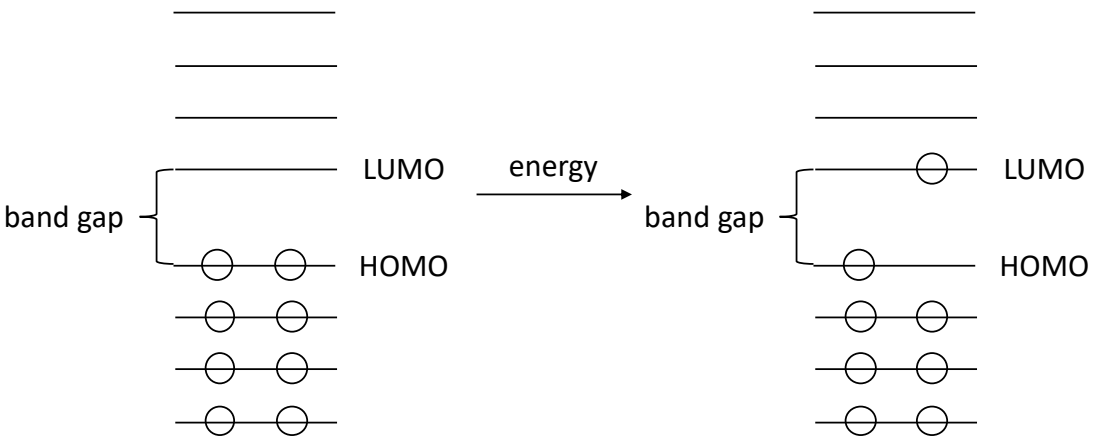

Figure 1.1. Generation of Carriers

In order to discuss conductance, it is necessary to talk about formation and transportation of carriers, *i.e.* electrons and holes. The formation of molecular orbitals will not be reviewed here, since it is the fundamental of organic chemistry. What should be noted is two molecular orbitals, the highest occupied molecular orbital (HOMO) and the lowest unoccupied molecular orbital (LUMO), which are analogous to the valence and conduction bands in inorganic band theory. Accordingly, the energetic gap between the HOMO and LUMO is called the band gap, the minimum energy input required to excite charge carriers into a conductive state. The conduction process can be divided into two steps as mentioned earlier. First, the generation of carriers can be described in Figure 1.1. When energy input, from thermal energy or solar energy, is larger than the band gap, an electron jumps from the HOMO to the LUMO level, leaving a hole behind and creating excitons, which will be further separated into free carriers. Next, the mobile carriers are transported so as to make currents flow, which is demonstrated in Figure 1.2 from Pope.[10] There are two kinds of mechanisms involved in carrier transport, and one is band transport (Figure 1.2a), the other is hopping transport (Figure 1.2b). The band transport mechanism applies to inorganic semiconductors, where electrons are delocalized. The hopping transport mechanism, nevertheless, is utilized in almost all organic semiconductors to transport charges from chain to chain. In this case, carriers can be localized and trapped within trap states along the backbone chains. Phonons, generated from lattice vibrations, are viable media to transport carriers between conjugated backbones.[11]

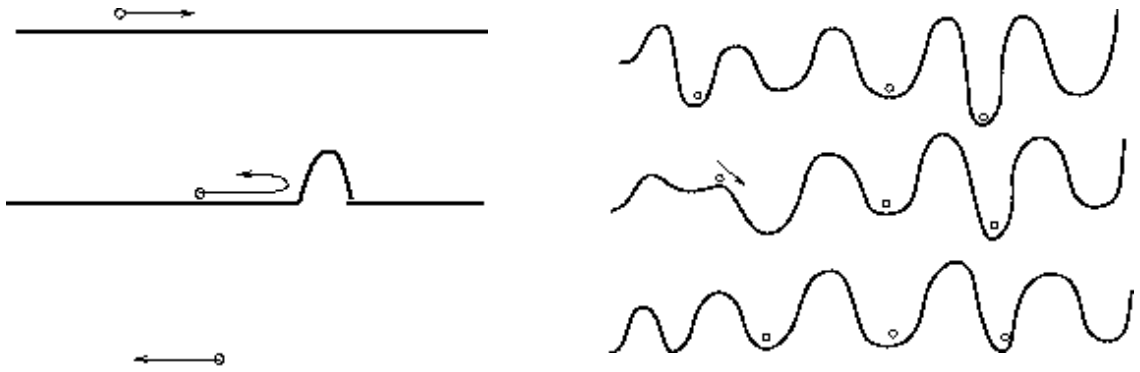

Figure 1.2. Transportation of Carriers, (a) Band Transport, (b) Hopping Transport[10]

1.3 CLASSIFICATION OF ORGANIC SEMICONDUCTORS

There are a variety of organic materials used for semiconductors but, generally, they can fall into one of three categories: p-type, n-type and ambipolar. P-type semiconductors, as the name suggests, are positive charge carrier transporting semiconductors, indicating the major carrier is hole. This kind of molecule usually has electron-donating group such as amino groups, serving as donor. The carrier in n-type semiconductors, however, is electron, and with electron-withdrawing groups like carbonyls attached to the backbone, these materials are more likely to accept electrons. Ambipolar semiconductors are more complicated as holes and electrons are both major carriers. In the following, some examples in these categories are given regarding conjugated polymers and small organic molecules.

1.3.1 *Polymer Conjugated Semiconductors*

Since the discovery of polyacetylene by Heeger *et al.*, conjugated polymers have been studied widely with the hope to find or design better materials, which are vital to the development of higher performance devices.[7] Poly(3-hexylthiophene) (P3HT, Figure 1.3a), poly(phenylene vinylenes) (PPVs, Figure 1.3b) are the most ubiquitous conjugated polymers, being used in organic field

effect transistors (OFETs), photovoltaics (OPVs) and light emitting diodes (OLEDs), among others.[12] The thiophene polymer semiconductors are of great interest because they have higher mobility in OFETs and tunability in crystallinity *via* side chain engineering. As a result of this, several thiophene family semiconductors are developed, such as poly(2,5-bis(2-thienyl)-thieno[3,2-b]thiophene)s (Figure 1.3c), poly(benzodithiophene)s (Figure 1.3d).[13] Apart from this, poly[2-methoxy-5-(2'-ethylhexyloxy)-p-phenylene vinylene] (MEH-PPV, Figure 1.3e) is also utilized as donor in bulk heterojunction polymer solar cells coupled with chemically modified C_{60} as the acceptor.[14]

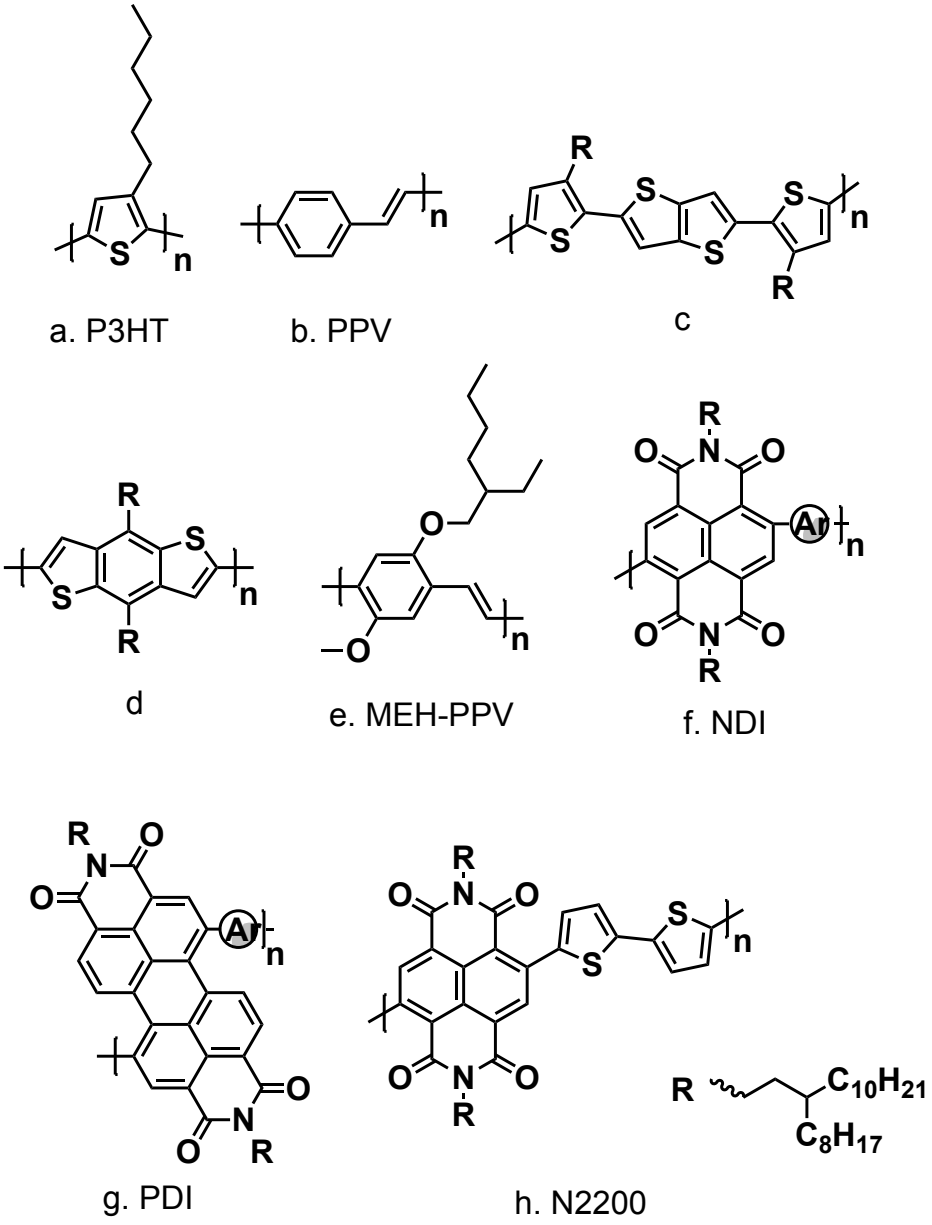

Figure 1.3. Structure of Conjugated Polymers

The above are all p-type semiconductors, and n-type semiconductors, nonetheless, are much more complex and rarer because of the lack of electron-withdrawing building block for n-type semiconductors.[15] Rylene diimide-based polymers, including naphthalene diimides (NDIs, Figure 1.3f) and perylene diimides (PDIs, Figure 1.3g), are the most popular ones being studied.[16] Among them, poly[N,N'-bis(2-octyldodecyl)-naphthalene-1,4,5,8-bis(dicarboximide)-2,6-diyl]-

alt-5,5'-(2,2'-bithiophene) (N2200, Figure 1.3h) reported by Watson *et al.* has not only satisfying performance in OFETs, the mobility of which can reach up to 0.85 $cm^2V^{-1}s^{-1}$ but also potential use in OPVs.[17]

1.3.2 *Small Molecule Organic Semiconductors*

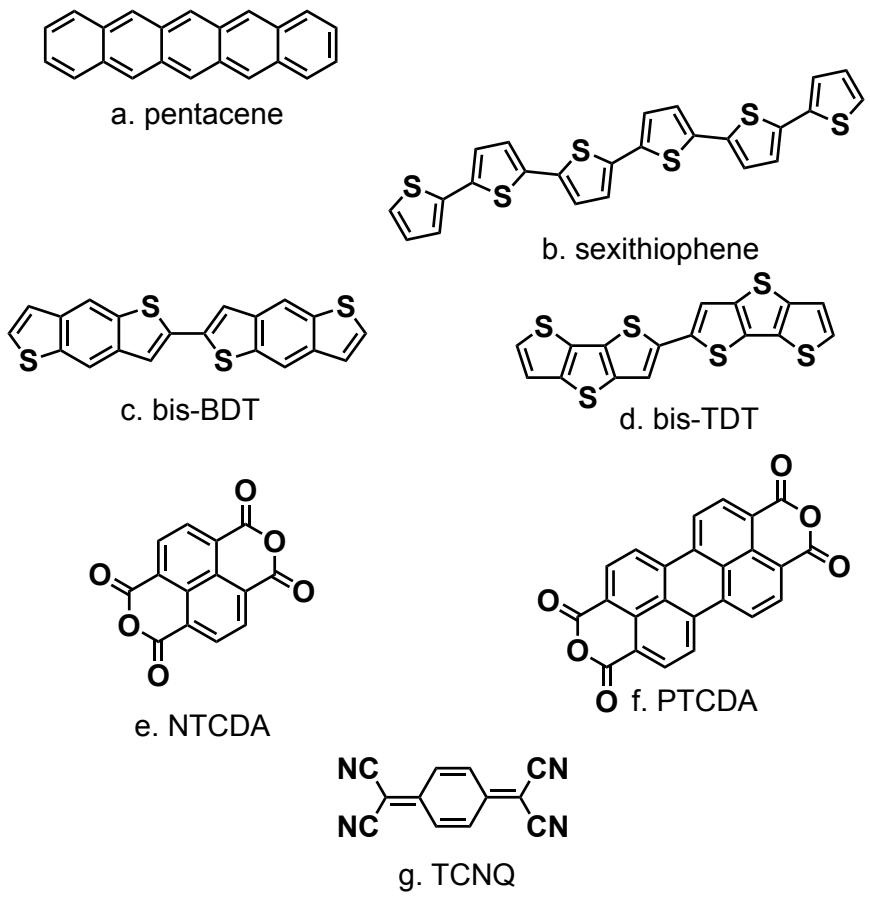

Figure 1.4. Structure of Small Molecule Organic Semiconductors

Compared to conjugated polymers, small organic semiconductors have negligible batch-to-batch variation in properties. Also, they are easy to purify after synthesis to obtain high purity materials, the key to higher crystallinity and better morphology, which results in higher mobility in OFETs.[18] Therefore, small molecules have the edge over polymer materials. For p-type materials, acenes and oligothiophenes are two classes of chemicals broadly used in the organic

semiconductor field, due to the fact that they have electron-rich structure and long conjugated length.[19] What's more, pentacene (Figure 1.4a), in the acene family, has better performance when making a comparison with others, whose mobility can reach up to 1.5 $cm^2V^{-1}s^{-1}$ in OFET devices.[20] Additionally, α-sexithiophene (6T, Figure 1.4b), from oligothiophene family, show mobility for 0.01-0.03 $cm^2V^{-1}s^{-1}$ in OFET.[21] Although the performance of 6T-based devices is not that promising, it helps to develop a series of derivatives, such as benzodithiophene (bis-BDT, Figure 1.4c) and thienodithiophene (bis-TDT, Figure 1.4d).[22, 23]

As mentioned previously, there are much fewer n-type materials than p-type ones. Thus, some examples frequently studied in this field are examined here to further the understanding. Rylene diimide-based small organic chemicals, including NDIs and PDIs, just like n-type polymer materials, are new-rising materials for substitution of non-fullerene acceptors in OPVs and other semiconductor devices such as OFETs.[15] For example, naphthalenetetracarboxylic dianhydride (NTCDA, Figure 1.4e) and perylenetetracarboxylic dianhydride (PTCDA, Figure 1.4f) based OFET devices have mobility of 0.002 $cm^2V^{-1}s^{-1}$ and 10^{-4} $cm^2V^{-1}s^{-1}$ respectively according to Laquindanum *et al.*.[24] Another example is tetracyanoquinodimethane (TCNQ, Figure 1.4g), proposed by Brown *et al.*, and it can be seen that n-type chemicals have one thing in common: they have many electron-withdrawing groups, which makes them good acceptors.[25]

1.4 Conclusion and Perspective

In this chapter, structure and classification of organic semiconductors are briefly discussed, and this is the foundation of comprehending electrical devices, such as OFETs, OPVs and OLEDs. In Section 1.2, the mechanism of carrier generation and transportation in organic semiconductors are emphasized, and some specific examples, especially small organic semiconductors are given in Section 1.3. Besides, it is worth noting that the shortage of n-type small organic chemicals, which

are urgently needed to make complementary OFET, is the reason studied extensively in this domain and the topic of this thesis, which will be clarified in the following chapters.[26]

Chapter 2. INTRODUCTION TO DEVICES AND CHARACTERIZATION METHODS

2.1 INTRODUCTION

As illustrated above, the invention and advancement of electrical devices are the biggest accomplishment of this century, and semiconductor devices, which are the most relevant to our daily life, are photovoltaics (PVs, Figure 2.1a) converting sunlight to electricity, light-emitting diodes (LEDs, Figure 2.1b) transforming electricity into light and field effect transistors (FETs, Figure 2.1c) forming core components of integrated circuits. Before moving on, the progression of these three devices made are recapped here to gain better insight.

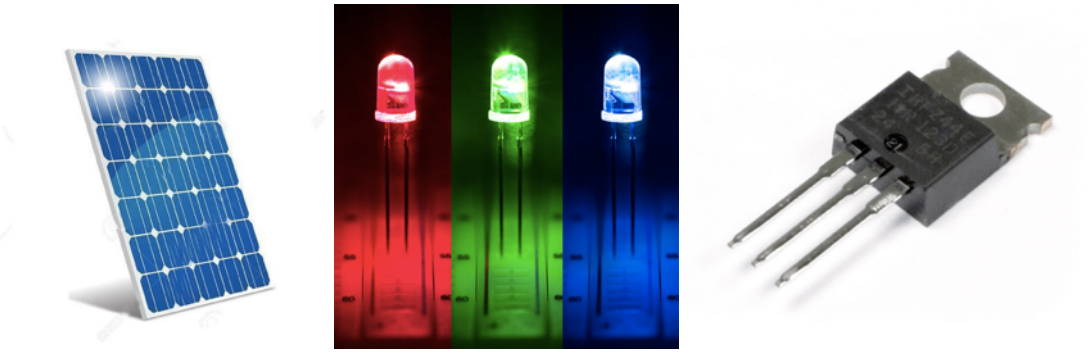

(a) (b) (c)

Figure 2.1. (a) PV from IndiaMART, (b) LED from Super Bright LEDs, (c) FET from Solarbotics

Photovoltaic devices, also known as solar cells, are commonly used on the rooftops to make use of the abundant and free solar energy, but most commercial solar panels are based on inorganic materials, silicon, because of their high power conversion efficiency (PCE). Organic photovoltaic devices (OPV), on the contrary, has relatively lower PCE compared to inorganic counterpart and is still being studied. The development of OPV can be divided into three parts. First, the structure of the initial OPV was quite simple: single-layer devices, with active materials being PPV and two

electrodes inserting, achieving PCE as low as 0.07%.[27, 28] Later, efficiency is enhanced to 1% when two-layer structure, one for p-type copper phthalocyanine and the other for n-type perylene tetracarboxylic derivative, is adopted by Tang.[8] At last, the bulk heterojunction structure, which is broadly utilized in this field, can reach to 2.9 % initiated by Heeger and Holmes.[29, 30] Now with PCE reaching up to 17.3%, the commercialization of OPV is just a matter of time.[31, 32] OLED has similar structure but reverse mechanism as OPV, and it involves the generation of three different colors, red, green and blue.[33] What is worth mentioning is that some commercialized OLED products have been manufactured, such as 55-inch OLED TV from LG Display, OLED display screen on phones from Apple and Samsung.[34] This indicates the transition from liquid crystal displays to OLEDs.

With respect to OFETs, metal-insulator-semiconductor diode was first reported by Ebisawa *et al.*, applying polyacetylene as semiconductor materials, which shows potential for field effect transistor.[35] Furthermore, the first OFET was fabricated by Tsumura *et al.* with polythiophene as active material, and the mobility was 10^{-5} $cm^2V^{-1}s^{-1}$ at that time.[36] The subsequent development of OFETs has been focused on materials design and fabrication process since the discovery of OPVs and OLEDs, and now the performance of OFETs, 11 $cm^2V^{-1}s^{-1}$ for electron mobility and up to 40 $cm^2V^{-1}s^{-1}$ for hole mobility, is close to industrial large-scale production.[37-40]

In this chapter, OFETs are the primary focus, and their structure, working mechanism will be discussed here. Also, methods to characterize properties of materials and performance of OFETs are talked about briefly. Lastly, a conclusion is made at the end of this chapter.

2.2 Organic Field Effect Transistors

OFETs, which are likely to be put into commercial application, such as flexible displays, sensors, wearable electronics and radio-frequency identification tags, are perfect substitutes for inorganic

silicon FETs due to their flexibility and tuneability as mentioned previously.[15] The problem, nonetheless, is the performance of devices, *i.e.* mobility of OFETs, which is still not enough to make commercial products. As a result of this, enhancing the performance of OFETs is the ultimate goal in this study. In this part, four common structures of OFETs and two working mechanisms, one for p-type, the other for n-type, are demonstrated to gain better understanding on OFETs.

2.2.1 *Structure of OFETs*

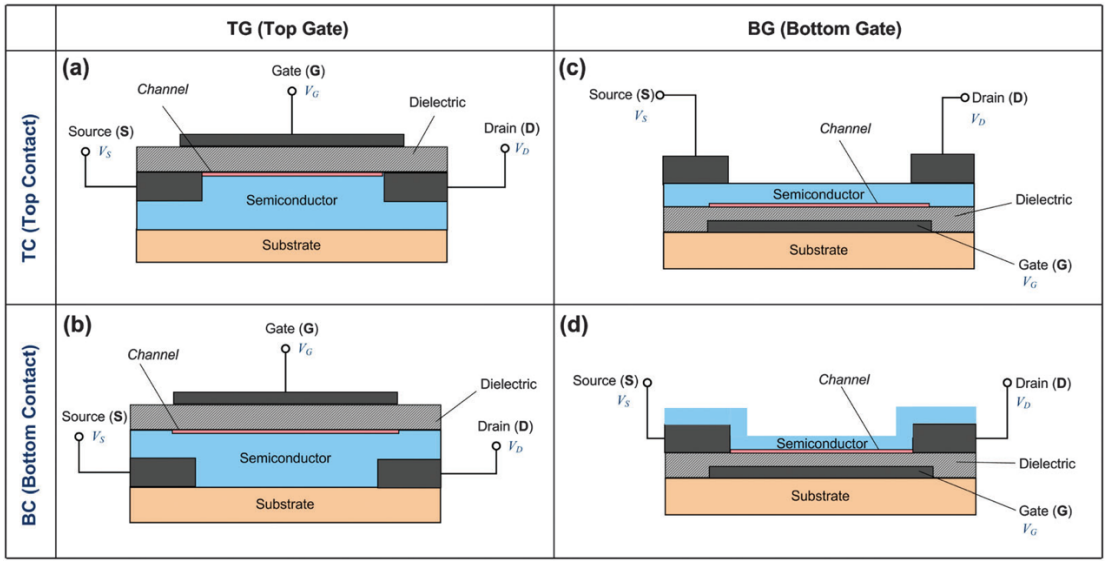

Figure 2.2. Four Structures of OFETs[41]

Before introducing structure of OFET, it is crucial to know core components making up of OFETs, such as the three electrodes – gate electrode, source electrode and drain electrode; substrate layer, dielectric layer and semiconductor layer. The specific function of these components will be mentioned in Section 0. Now we focus on OFET structures, and there are four different structures in fabricating OFETs: top gate, top contact (TGTC, Figure 2.2a); top gate, bottom contact (TGBC, Figure 2.2b); bottom gate, top contact (BGTC, Figure 2.2c); bottom gate, bottom contact (BGBC, Figure 2.2d). Among them, BGTC structure will be employed during my research study since it is the easiest one to fabricate. Next, these four structures will be discussed one by one.

First, top gate structure is considered. TGTC structure, as name suggests, is where gate electrode is at the top, source and drain electrodes are under dielectric layer. Different from this is TGBC structure, where gate electrode is still at the top, but source and drain electrodes are under semiconductor layer. The advantage of adopting top gate structure lies in that gate electrode and dielectric layer protects semiconductor layer from exposing to the air in the environment, contributing to better performance in mobility and stability, and this kind of structure suits for n-type OFET because it will decrease the trapping and annihilation of carrier electrons.[15] However, the disadvantages are the difficulty to fabricate devices and lower mobility caused by uneven surface of semiconductor layer.[41]

Another kind of structure is bottom gate OFET, which is more prevalent compared to top gate structure. This is because the doped silicon wafer acting as gate electrode with thermally grown SiO_2 as dielectric layer is accessible by purchasing from manufacturers. What's more, the even surface of the wafer makes it effortless to deposit semiconductor layers after cleaning, reducing discontinuity of active materials in this layer. The drawback, nevertheless, is that the materials for gate electrode and dielectric layer are fixed, so it seems implausible to use other materials as gate electrode and dielectric layer.[41]

2.2.2 *Working Mechanism of OFETs*

The working principles of OFETs are crucial in calculating performance of OFETs, including mobility, current on/off ratio and threshold voltage, thus great care should be taken to understand them in this section. As we know, there are three kinds of OFETs: p-type OFET, n-type OFET and ambipolar OFET. Since three classes of semiconducting materials have explained earlier, it is straightforward to figure out these three devices. The major carrier in p-type OFET is hole, and the active material is p-type chemical; in n-type OFET, the electron conducts the device, and n-

type semiconductor is the active layer; both hole and electron contribute to the conductance of ambipolar OFET, and ambipolar material serves as semiconductor layer. Among them, the performance of n-type OFETs is still behind p-type ones due to lack of materials, trapping and annihilation of electrons.[15] The mechanisms of p-type and n-type OFETs will both be discussed in this part.

Take BGTC structure (Figure 2.2c) for example, the channel formed on the top of dielectric layer in the semiconductor layer is the main passage to conduct carrier, and source and drain electrodes connect to the channel, making the flow of carriers possible. Additionally, the formation of the channel is closely related to gate electrode and dielectric layer, constructing a capacitor-like structure. Hence, when gate electrode is biased, a sheet of channel will be induced on the surface of dielectric layer, and this channel is the main reason why the device is working.[40]

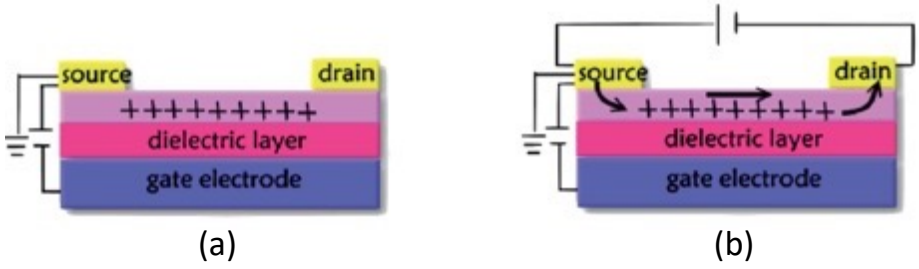

Figure 2.3. Working Mechanism of P-type OFET, (a) Without Drain Voltage, (b) With Drain Voltage[42]

For p-type OFET, when there is no voltage applied to gate electrode, the device is at ‘OFF’ status, meaning little or no current will flow, even when applying voltage to the source and drain electrodes due to low concentration of hole carriers in the semiconductor layer. Normally the source electrode is grounded, so if a negative voltage is applied to the gate electrode, the semiconductor layer will induce holes in the channel as exhibited in Figure 2.3a to switch the device to ‘ON’ status. Another thing to be kept in mind is that the gate voltage should be higher

than the threshold voltage in order to turn on the device due to the fact that some induced holes are trapped in the active layer, preventing them from moving.[42] With gate voltage higher than threshold voltage, when the voltage between source electrode and drain electrode is negative, holes are injected from source electrode and flow to drain electrode *via* the electrical field established between source and drain electrodes (Figure 2.3b). This is how p-type OFET devices conducts currents.

As regards n-type OFET, it is similar to p-type OFET, but the difference is that positive voltage is applied to the gate electrode so that electrons can be induced at the interface of semiconductor layer and dielectric layer. Additionally, positive voltage is applied between source and drain electrodes, so the source electrode, in this case, injects electrons into the channel, and electron carriers are transported to the drain electrode.

2.3 CHARACTERIZATION METHODS

Characterization, determining the properties of materials and performance of devices, makes a big difference to the research direction of our study. There are various characterization methods nowadays, and it is impossible to clarify all of them in this part. According to our research, two aspects will be explained here, one is materials characterization, including cyclic voltammetry (CV) and Ultraviolet-visible spectroscopy (UV-Vis), and the other is OFET devices characterization, such as mobility, on/off ratio and threshold voltage.

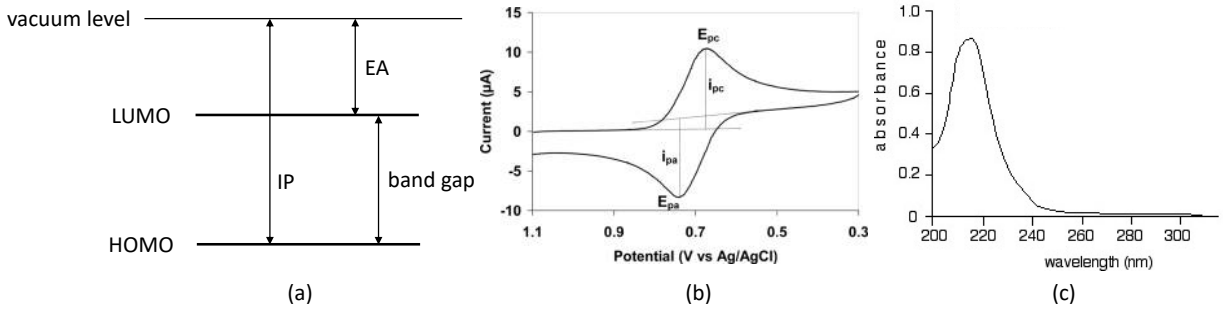

Figure 2.4. Characterization of Materials, (a) Energy Diagram, (b) CV Curve from Wikipedia, (c) UV-Vis Spectrum from Chemguide

CV is an electrochemical method to determine HOMO level and LUMO level of materials, the important electrical properties demonstrated in Chapter 1. The energy of HOMO is related to ionization potential (IP), the minimum energy required to remove one electron from the frontier, HOMO level to vacuum level, so IP = E_{vacuum} - E_{HOMO}. In the same manner, the relationship between LUMO level and electron affinity (EA), the energy released to add an electron into LUMO level from vacuum level, is EA = E_{vacuum} – E_{LUMO}. Their relationship has been drawn in Figure 2.4a to better apprehend. CV characterization will undergo oxidation process and reduction process, and energy consumed or released during these two processes is described by the IP and EA respectively.[43] Consequently, the HOMO level and LUMO level can be estimated by E_{ox} and E_{red} measured by CV, and the typical CV curve is shown in Figure 2.4b. UV-Vis, in fact, can only evaluate the band gap of materials by excitation of electrons from HOMO level to LUMO level under illumination of light at energy greater than or equal to the band gap. The typical result diagram is illustrated in Figure 2.4c. When assessing materials for OFET application, UV-vis characterization is often exploited to verify the results from CV. It is also used to examine intermolecular, intramolecular forces and vibronic structure.[44, 45]

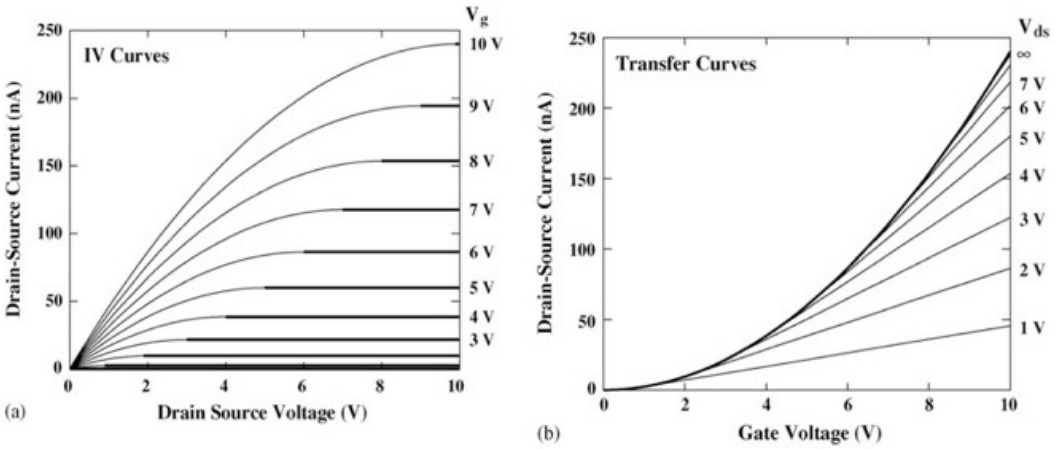

Figure 2.5. I-V Curves for Characterizing OFET, (a) Output Curve, (b) Transfer Curve[46]

As for OFET device characterization, three parameters are concerned in this study: mobility, on/off ratio and threshold voltage, which can be extracted from the current-voltage curve (I-V curve). There are two types of I-V curves commonly used in characterizing OFETs, one is the output curve (Figure 2.5a), which is generated by fixing gate voltage (V_G) and sweeping drain-source voltage (V_{DS}), the other is the transfer curve (Figure 2.5b), which is measured by by fixing V_{DS} and sweeping V_G. From the output curve, two regions are presented in the figure, linear region and saturation region marking with bold lines in Figure 2.5a. Aforementioned mechanisms indicate that when the device is at 'ON' status, V_G is higher than threshold voltage (V_T). Keeping the V_G at a constant value, and increasing V_{DS}, the current flowing from source to drain (I_{DS}) also builds up as a result of a larger voltage difference until V_{DS} reaches a specific point, where "pinch off" happens. This marks the transition to the saturation region, and I_{DS} remains maximum, resulting from the closure on one side of the device.[47] The conditional value for V_{DS} is correlated to V_G and V_T, so if $V_{DS} < V_G - V_T$, it is in linear regime, and if $V_{DS} > V_G - V_T$, it stays in saturation regime.[40] For transfer curve, it is usually utilized to compute performance of devices. Mobility can be calculated from the transfer curve, but two mobilities can account for conductance of

OFETs, one in linear regime, *i.e.* linear mobility, the other in saturation regime, *i.e.* saturation mobility. In linear regime:

$$I_D = \frac{W}{L} C\mu (V_G - V_T - \frac{V_D}{2}) V_D, V_D < V_G - V_T \tag{2.1}$$

where C is the capacitance of dielectric material, W is the width of the channel, L is the length of the channel, μ stands for linear mobility. However, in saturation regime:

$$I_{D,sat} = \frac{W}{2L} C\mu (V_G - V_T)^2, V_D > V_G - V_T \tag{2.2}$$

$$\sqrt{I_{D,sat}} = \sqrt{\frac{W}{2L} C\mu} (V_G - V_T) \tag{2.3}$$

where μ is saturation mobility, and the others are the same as above.[48] Furthermore, saturation mobility is the most acceptable results when comparing performance of OFETs, so it will be used in our study.[41] Threshold voltage can also be inferred by extrapolating linear plots of $\sqrt{I_D}$ - V_G to x axis. On/off ratio is another important parameter to evaluate OFETs, and it is the ratio of drain current when the device is at 'ON' status to 'OFF' status, reading directly from transfer curve. This parameter reflects the sensitivity and responsivity of OFETs, thus the larger, the better.

2.4 CONCLUSION

In this chapter, concentration has been focused on devices, OFETs, and almost all aspects have been included, such as structure, classification, operation principles and characterization methods of OFETs. The reason to choose bottom gate, top contact structure as our OFET device is explained, and the working mechanism of n-type OFETs, our research topic, is also clarified. Further, three characterization methods, two for materials (CV and UV-Vis) and one for devices (I-V curves) are illustrated in detail and approaches to derive three parameters (mobility, threshold

voltage and on/off ratio) from transfer curve by I-V are also shown. The next chapter will frequently use the practice described here to characterize self-made OFETs.

Apart from materials design and synthesis, modifying and expanding the structure of OFETs are other ways to advance the development of OFET devices. Some other options include trying to improve the surface energy of the dielectric layer with self-assembled monolayers (SAMs), or to substitute the inorganic SiO_2 dielectric layer with organic and polymer insulators in the hope of obtaining better performance.[49, 50] Given these, there still remains possibility for amelioration and growth of OFETs, and commercialization is just around the corner.

Chapter 3. FABRICATION AND CHARACTERIZATION OF N-TYPE OFET BASED ON SYNTHETIC CAFFEINE DERIVATIVES BY C-H ACTIVATION

3.1 INTRODUCTION

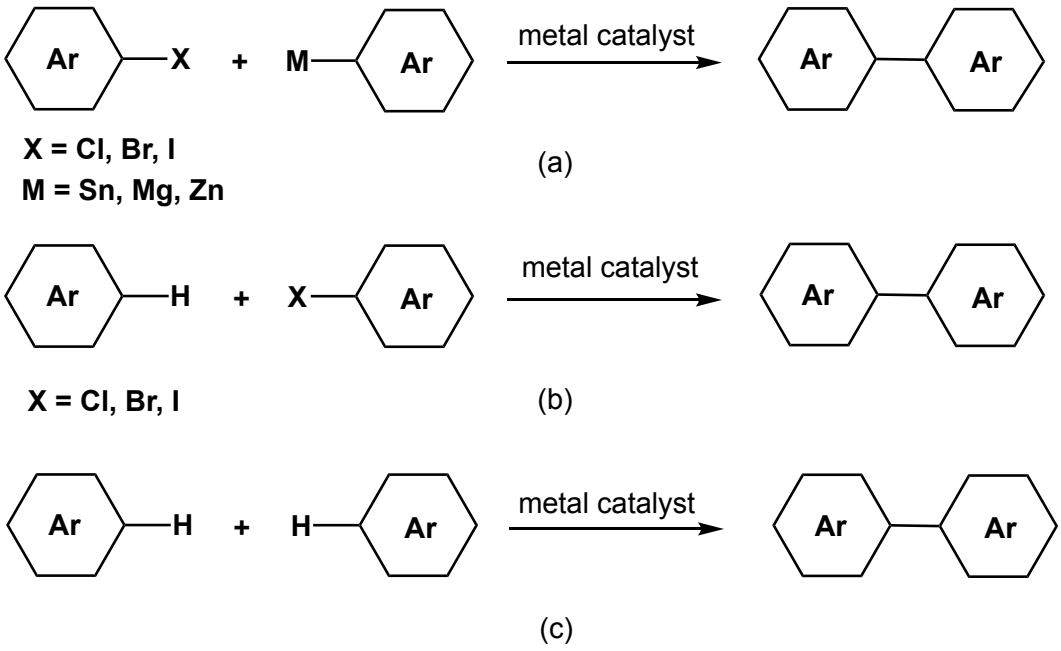

Figure 3.1. Formation of Aryl-Aryl Bonds, (a) Traditional Cross-coupling Reaction, (b) C-H/C-X Activation, (c) Oxidative C-H Activation

Organic semiconductors, as introduced in the Chapter 1, are one class of materials with extended π-conjugated systems. With the aim to construct backbones with longer conjugation lengths, the easiest solution is to join different semiconducting chemicals together with conjugated carbon-carbon (C-C) bond. One way to achieve this is to create aryl-aryl (Ar-Ar) systems.[51] In this way, LUMO level can be lowered and HOMO level can be raised. As a result, the performance and stability of devices will be improved. Several experimental methods have been established to form Ar-Ar bonds between two aromatic compounds, including Kharasch reaction, Negishi reaction,

Stille reaction, Suzuki reaction and C-H activation. For traditional cross-coupling reactions (Figure 3.1a), the first four reactions, they are usually achieved by utilizing metal catalysts, nickel or palladium, demonstrating promising efficiency and generality.[52] Widely accepted as these reactions are, some major problems exist, which slows down the study of cross-coupling reactions. First, most molecular substrates need pre-functionalization, a time-consuming and tiresome procedure, to activate these reactants.[32] Secondly, the pre-functionalization process sometimes is a little difficult to accomplish because some organometallic reagents have relatively low stability.[53] Lastly, some byproducts that are harmful and detrimental to the ecosystem are produced during the cross-coupling reaction. Accordingly, a simpler, more reliable, and greener approach has been developed, which is known as C-H activation.

As illustrated in Figure 3.1 b and c, direct C-H arylation increases atom utilization and avoids the production of toxic heavy metal pollution to the environment, compared with traditional cross-coupling reactions. Hence, this method has attracted increased attention into synthesis of natural products, pharmaceuticals and electronic materials.[51, 54-56] There are, in fact, two types of C-H activation under development. One is C-H/C-X type arylation, which involves halogen atom. The other is C-H/C-H type arylation or called oxidative C-H activation since it requires oxidant to make reactions happen.[57] The latter reaction, nevertheless, is more thermodynamically unfavorable given inertness of aromatic C-H bond compared to C-X and C-M bonds. As a result, this kind of reaction requires harsh condition to overcome reaction energy barrier and it has poor selectivity.[53, 58] As a result of this, our focus will be on C-H/C-X type arylation, which is the main synthetic method used in this study. For this class of reaction, several transition metal catalysts have been applied to this system, and the most popular one is palladium catalyst, which has been extensively studied in this field due to its high conversion and availability. Among them, the origin

of palladium catalyzed C-H activation is reported by Fujiwara *et al.* to arylate olefins by utilizing palladium acetate.[59] After that, the palladium catalyst system becomes sounder, with electron-rich phosphine triphenylphosphine (PPh_3) as a ligand and cesium carbonate (Cs_2CO_3) as base, and the reaction typically progresses overnight at over 100 °C to accomplish the conversion.[60] Another important problem associated with C-H activation is regioselectivity, and luckily with the help of directing groups, specific sites of electrically neutral arene reactants can be selected to achieve desired products.[57]

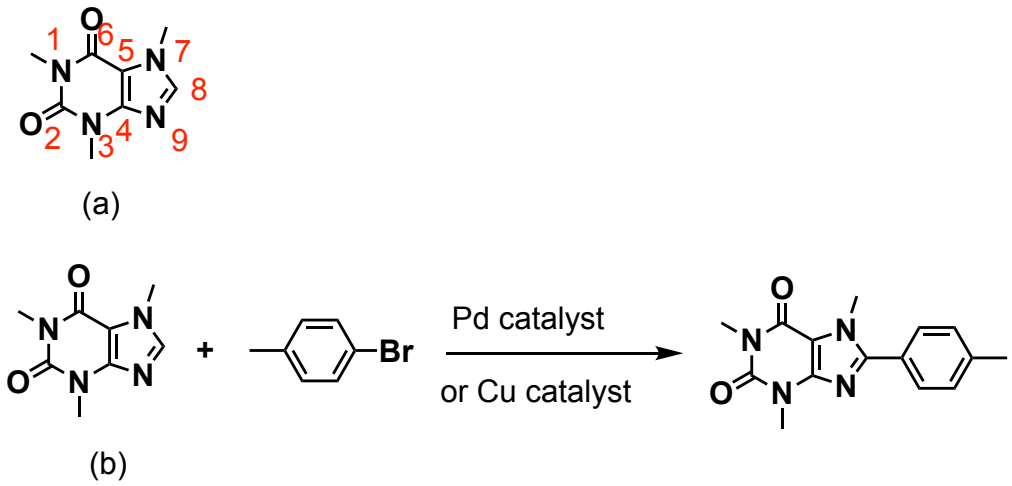

Figure 3.2. Caffeine Structure (a) and Application (b)

Next, we will talk about the essential component of our semiconductor materials, caffeine molecules (Figure 3.2a). Caffeine belongs to xanthine family, which are biologically active materials; other compounds in this family include theophylline and theobromine. Most studies on xanthine derivatives relate to biology and medicine, like for A_1- and A_2- adenosine receptors antagonists and antagonists at A_{2B} adenosine receptors.[61, 62] Furthermore, Zhao *et al.* reported direct arylation of caffeine derivatives with benzene employing palladium acetate and copper iodide respectively (Figure 3.2b).[63, 64] There is no literature on synthesizing caffeine derivatives as electrical semiconductors. Additionally, the caffeine molecule is a potential electron acceptor

since two carbonyl groups acting as electron-withdrawing groups attached to the purine ring, making it electron-deficient, which results in higher mobility and stability of N-type OFET. Additionally, alkyl substituents of caffeine molecules can better the solubility and intermolecular packing of products, thus hydrogens attached to 1-N position are replaced by alkyl chains.[18] Besides, in order to extend π-π electrons, benzene and thiophene functioning as electron donor are introduced into the caffeine molecules. This not only increases the conjugation length of the organic molecule, but also constructs an acceptor-donor-acceptor (A-D-A) structure, which is more likely to be self-assembled due to charge-transfer interactions between donor and acceptor.[65] Last but not least, A-D-A structure has high symmetry if two acceptors are the same, which indicates it has high crystallinity, so high charge transport will be reached by establishing A-D-A structure.

In this chapter, caffeine derivatives with different side chains are synthesized by C-H activation using palladium catalyst, and nuclear magnetic resonance (NMR), UV-Vis, CV results are also discussed here. N-type OFET devices are fabricated using two caffeine derivatives to explore the impact of side chains on the performance of devices.

3.2 RESULTS AND DISCUSSION

3.2.1 *Caffeine Derivatives Synthesis*

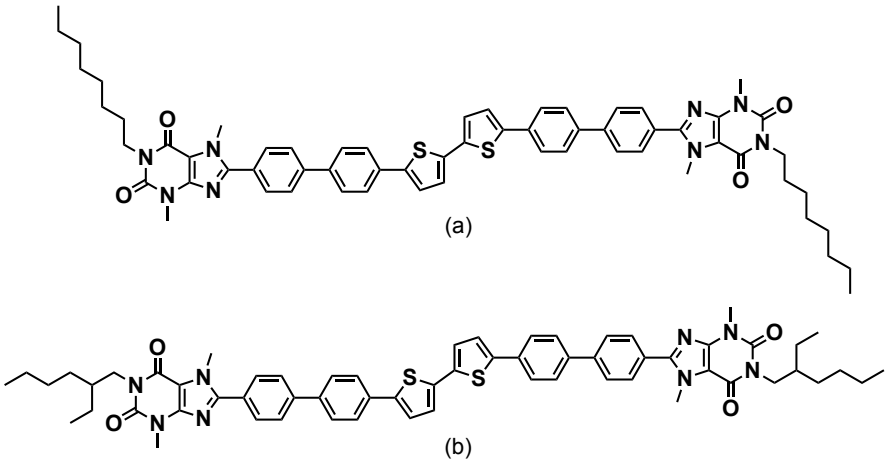

Figure 3.3. Final Products, (a) **TP2OT**, (b) **TP2EHT**

As briefly discussed in Section 3.1, the final organic semiconductor products are shown in Figure 3.3, and one is linear chain substitute at 1-N position of theobromine, bithiophene-tetraphenyl-di(octyl-theobromine) (**TP2OT**, Figure 3.3a), the other is side-chain substituted at the same position, bithiophene-tetraphenyl-di(ethylhexyl-theobromine) (**TP2EHT**, Figure 3.3b). The benefits of designing such long and symmetric chains was discussed above, so now the discussion will focus on synthetic routes.

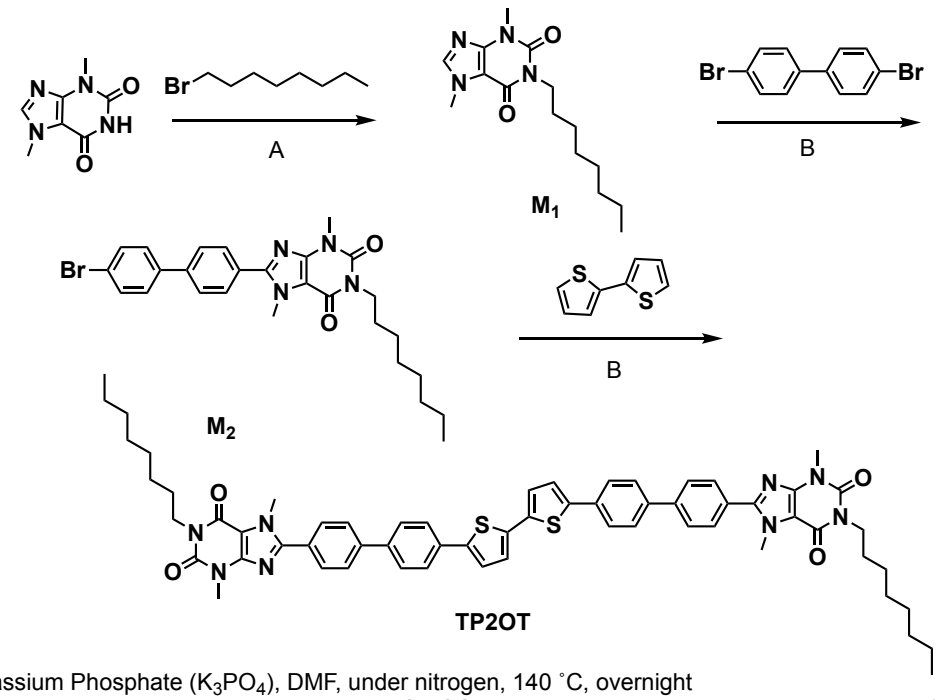

A: Tripotassium Phosphate (K_3PO_4), DMF, under nitrogen, 140 ˚C, overnight
B: $Pd_2(dba)_3$, Tris(2-methoxyphenyl)phosphine, Cs_2CO_3, Pivalic acid, Toluene, under nitrogen, 110 ˚C, overnight

Figure 3.4. Procedures to Synthesize Linear Product, **TP2OT**

The procedures to make **TP2OT** are demonstrated in Figure 3.4, and this is a three-step reaction involving bimolecular nucleophilic substitution (S_N2) and C-H activation. In the first step, from theobromine molecule as starting material, which is available and cheap to purchase, to **M1** is S_N2 process, and tripotassium phosphate (K_3PO_4) is an important base in deprotonation during this reaction. As a matter of fact, K_3PO_4 is widely employed in food industry, phosphate buffer solutions and organic synthesis because of its excellent solubility in organic solvents and non-nucleophilic property.[66] Consequently, the N-H bond at 1-N position is deprotonated by K_3PO_4, which is highly possible considering the two electron-withdrawing groups, carbonyls, at 2-, 6-position. This makes the caffeine molecule a nucleophile, attacking electropositive octyl-bromide with electronegative halide atom attached, giving rise to the formation of **M1**. The next two steps are similar, with the same reaction conditions adapted from literature for palladium catalyzed C-H activation.[51, 63] Previously, regioselectivity is examined, and it is critical to form desired C-C

bonds to obtain targeted products. This problem can be solved by creating electron-deficient sites or directing groups, like in **M1**, the only available spot in a purine ring is 8-C position, so C-H activation will happen at that site, which indicates high selectivity. The last step, direct arylation takes place at 5- and 5'- position, and this is due to relatively more reactive α-positions of thiophene rings. What should also be mentioned is that the ratio of **M2** to bithiophene is 2 to 1, ensuring both 5- and 5'- position are taken during the reaction so that **TP2OT** is successfully synthesized, the NMR spectrum of which is illustrated in Chapter 5. Although *via* thin layer chromatography (TLC) after the reaction, some one side substituted byproducts are identified, the desired products can be purified through column chromatography.

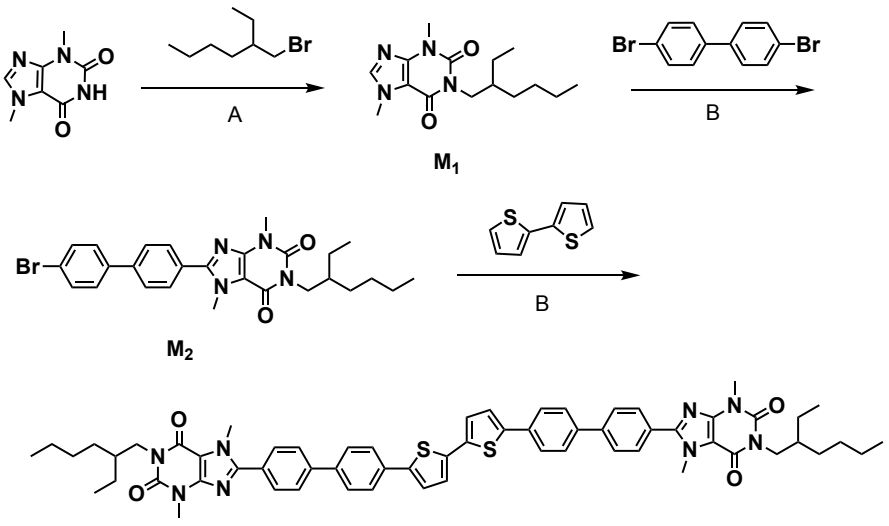

A: Tripotassium Phosphate (K_3PO_4), DMF, under nitrogen, 140 ˚C, overnight
B: $Pd_2(dba)_3$, Tris(2-methoxyphenyl)phosphine, Cs_2CO_3, Pivalic acid, Toluene, under nitrogen, 110 ˚C, overnight

Figure 3.5. Procedures to Synthesize Side-chain Product, **TP2EHT**

For the synthesis of **TP2EHT** (synthesis steps in Figure 3.5), one can utilize a similar approach, but the only difference is the haloalkane, which is 2-ethylhexyl bromide in this case. Also, since branched a side-chain is presented in the product, the solubility of **TP2EHT** is better than **TP2OT**, producing high concentration solution, which might be helpful in enhancing performance of devices. The NMR spectrum of **TP2EHT** is included in Chapter 5.

3.2.2 *Optical and Electrochemical Properties*

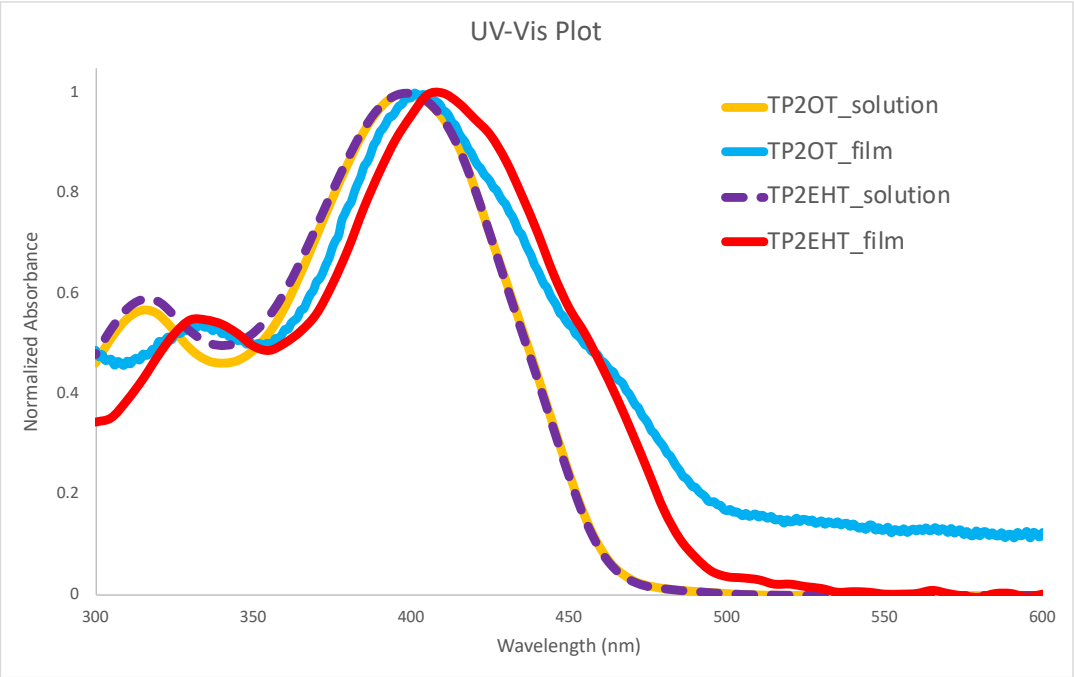

Figure 3.6. UV-Vis Spectroscopy

The optical property, absorption in this context, was determined by UV-Vis, and results are in Figure 3.6, which covers absorption spectrum of **TP2OT** and **TP2EHT** in both solution (chloroform) and solid (thin film) state. Moreover, onset points of absorption spectrum can be read from the plots, and optical band gap can be calculated by using equation:

$$E_{g,opt} = \frac{1240}{\lambda_{onset}(nm)}(eV) \tag{3.1}$$

Computation results are summarized in Table 3.1. From the figure and table, it can be seen clearly that for both **TP2OT** and **TP2EHT**, the onset absorption is red-shifted from solution to thin film state, and this is related to the aggregation of molecules. In solid state, the molecule is closely packed so that J-aggregate is formed in this case, which lowers band gap of the semiconductor materials.[67] Another thing should be noticed is that the plots almost overlap with each other in solution, and this can be explained by large intermolecular distance in solution and the little

electronic variation introduced by different alkyl sidechains. On the other hand, in solid state, the band gap of **TP2OT** is slightly smaller than **TP2EHT**, and branched side chain plays an important role in this influence. The packing of **TP2EHT** is not that compact as **TP2OT** because of steric effect caused by branched chain on **TP2EHT**, resulting in less aggregated and larger band gap.

Table 3.1. Optical and Electrochemical Properties of Caffeine Derivatives

Caffeine Derivatives	λ_{onset}/nm		$E_{g,\ opt}$/eV	E_{ox}/HOMO /eV	E_{red}/LUMO /eV	E_g/eV
	solution	film				
TP2OT	463	498	2.49	1.09/-5.89	-1.84/-2.96	2.93
TP2EHT	465	495	2.51	0.97/-5.77	-1.71/-3.09	2.68

CV, characterization method introduced in the previous chapter, was exploited to measure HOMO level and LUMO level of materials, and results are also exhibited in Table 3.1. In n-type OFET, we are more concerned about LUMO level since electrons are injected into this energy level. By comparing to the work function of common metals (Table 3.2), active metal, such as barium and calcium, seems to be a good choice for OFET electrodes due to proximity of their work function to the LUMO energy level of caffeine derivatives. However, silver was chosen as electrodes in this study instead of active metals to better control fabrication process. Furthermore, if optical band gap (from UV-Vis) and electronic band gap (from CV) are contrasted with each other, optical band gap is typically lower than electronic band gap, which is in accord with theory. The theory states that when an electron is excited from HOMO level to LUMO level by absorbing energy, electron-hole pair is still bound to each other, while by electrochemistry, this bond is broken, and electron and hole become free carriers.[68] As a result of this, band gap measured by UV-Vis is generally smaller than the one obtained using CV. At last, the comparison between **TP2OT** and **TP2EHT** is also made in order to clarify the influence of branched side chain have on properties of materials. From the table, the band gap of **TP2OT** is larger than **TP2EHT**, in

conflict with the relationship they possessed from UV-Vis measurement, which is commonly observed in conjugated polymers.

Table 3.2. Work Function of Common Metals[69]

Metals	Work Function/eV	Metals	Work Function/eV
Ag	4.26 – 4.74	Au	5.10 – 5.47
Al	4.06 – 4.26	Cu	4.53 – 5.10
Ba	2.52 – 2.70	Ca	2.87

3.2.3 *OFET Mobility Characterization*

To characterize performance of OFET devices based on caffeine derivatives **TP2OT** and **TP2EHT**, BGTC was chosen as the device architecture as explained earlier, and spin coating was used to form the semiconductor active layer in the OFET device. Unfortunately, after several attempts, the devices did not seem to work at all, which was implied by the low drain current ($I_d < 10^{-9}$ A) and curves not indicative of n-type OFET characteristic. Herein, these attempts are listed for further discussion.

On one hand, the solvent to dissolve caffeine derivatives was explored, and two solvents, chlorobenzene and chloroform, were examined. It turns out that caffeine derivatives have better solubility in chloroform than chlorobenzene, but solubility in chloroform is still limited. For **TP2OT**, the concentration in chloroform can only reach up to 1 mg/ml because of long conjugation carbon backbones. For **TP2EHT**, the concentration increases to 5 mg/ml as expected due to larger interchain distance. This makes it easier for solvents go through and dissolve compounds. However, the incompact packing of **TP2EHT** lowers crystallinity, which might lead to poor performance. As a result, chloroform was chosen as the solvent, given higher solubility and less residues, which often gives rise to better film morphology after spin coating. What's more, considering low concentration of the solution, different spin coating speeds were investigated to

optimize thickness of active layer. The more quickly the spin coater rotates, the thinner the film is, so by adjusting the speed, desired thickness of semiconductor film can be achieved. Two speeds were tried in this experiment, 2000 rpm and 1000 rpm respectively, but none of them showed satisfying results.

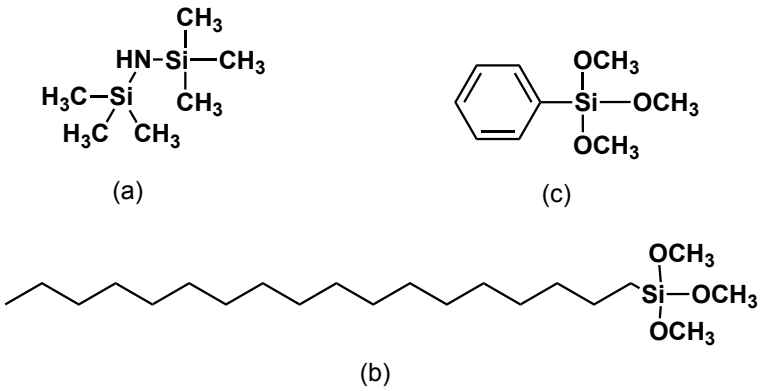

Figure 3.7. Structure of SAMs, (a) HMDS, (b) OTMS, (c) PTS

On the other hand, we can optimize the surface in an effort to improve interfacial contact and reduce leakage current between the dielectric and semiconductor.[70] A self-assembled monolayer (SAM) is often the best choice to modify surface of substrate. Therefore, in this experiment, three SAMs, including hexamethyldisilazane (HMDS, Figure 3.7a), octadecyltrimethoxysilane (OTMS, Figure 3.7b) and phenyltrimethoxysilane (PTS, Figure 3.7c), were tested to make substrate surface hydrophobic, which makes the surface more compatible with organic semiconductors.[49, 71, 72] The results indicated that HMDS-treated substrate was fully covered with SAM and the most consistent one with each batch, and PTS-treated one had the least coverage, which might be related to treatment methods. For HMDS, spin coating was exploited to deposit SAM, and it covered the whole surface of the substrate. For PTS, solution deposition and spin coating were both tried, but only part of the surface was covered with SAM. Another approach researched was to blend insulating polymer with semiconductor materials, which expected to make small organic semiconductors migrate to the surface of the polymer matrix, allowing the formation of better

contact and morphology.[73, 74] Hence, polystyrene (PS) is serving as insulating polymer during the fabrication, and two ratios are investigated, *i.e.* caffeine derivative: PS = 1:1 and 2:1. By annealing at 100 °C for about 15 min after fabrication process, performance of OFET devices is characterized, the mobility of these two devices based on small organic molecule-polymer blended materials, however, doesn't have much improvement.

3.3 CONCLUSIONS

Two caffeine derivatives, **TP2OT** and **TP2EHT**, have been successfully synthesized by C-H activation catalyzed by palladium-phosphine system, which can be confirmed by NMR spectrum in Chapter 5. Furthermore, different characterization methods on both materials, such as UV-Vis, CV and OFET devices, the mobility, threshold voltage and on/off ratio, are measured in this study. The optical and electrochemical properties of **TP2OT** and **TP2EHT** are compared to examine the impact of branched side-chain on the properties of caffeine derivatives. The experiment on OFET devices, on the other hand, is not that satisfying since none has shown the feature of working n-type OFET. As discussed above, the problem comes from a variety of aspects, such as molecular structure of caffeine derivatives, process conditions for fabrication and interfacial contact between semiconductor and insulator.[37]

Chapter 4. CONCLUSIONS AND FUTURE WORK

In conclusion, this thesis focuses on synthesis of organic semiconductors and their application in OFETs. In Chapter 1, organic semiconducting materials, both small organic molecules and polymers, are briefly talked about with concentration on n-type small organic molecules. Some examples are given and reasons why n-type semiconductors are lacking and in desperate need of are also discussed. In Chapter 2, attention has shifted to semiconducting devices, including OPV, OLED and OFET, and most of the time has been spent on demonstrating OFET devices, such as structure, mechanism and characterization methods. These two chapters are some fundamental knowledge, laying a foundation for further discussion of our work. Chapter 3, the most important chapter, manifests all of my research. In this chapter, two caffeine derivatives, **TP2OT** and **TP2EHT**, are successfully synthesized by green, efficient C-H activation. Optical property, electrochemical property and performance are characterized by different approaches to investigate the difference between these two semiconductor molecules, although n-type OFET devices fabricated show unsatisfactory performance.

The next step for this study can be divided into two parts. First, for devices, single-crystal OFET devices can be considered as last attempt for **TP2OT** and **TP2EHT**, and the reason is that single-crystal OFET usually has very high mobility compared to thin-film OFET due to better chain orientation and high purity of semiconductors.[75] Therefore, if single-crystal OFETs utilizing caffeine derivatives as semiconductor layers still exhibit low or no mobility, these two molecules are not suitable for OFET devices. Second, for molecules, extending conjugated backbones to increase conjugated length and finding new building blocks for N-type OFET are alternatives in terms of synthesis. Inserting rylene diimide-based small organics, NDIs and PDIs,

for example, makes main carbon backbone more electron-deficient is another practice to find a way out.

Chapter 5. SUPPORTING INFORMATION

5.1 MATERIALS AND INSTRUMENTS

All solvents and reagents were purchased from Sigma-Aldrich, except 2,2′-bithiophene was purchasd from Matrix Scientific, octadecyltrimethoxysilane (OTMS) was purchased from TCI America. They were all used without further purification. Silica gel was purchased from Millipore Sigma (porosity: 60Å).

^{1}H-NMR spectra were obtained using Bruker AV-500 spectrometer. UV-Vis absorption spectra were recorded on Perkin-Elmer Lambda 950 - UV Vis/NIR spectrophotometer. Cyclic Voltammetry (CV) was conducted on CHI660E electrochemical workstation from CH Instruments, Inc with 0.1 M tetrabutylammonium hexafluorophosphate in anhydrous acetonitrile as electrolyte. Carbon was used as working electrode; platinum wire was served as counter electrode and $Ag/AgNO_3$ was worked as reference electrode. Characterization of OFETs was performed on Signatone Probe Station with HP4145B semiconductor parameter analyzer controlled by LabVIEW codes. The fabrication and characterization process were carried out in nitrogen glovebox.

5.2 SYNTHETIC DETAILS

All reactions were performed under atmosphere of nitrogen utilizing standard Schlenk line technique. The reaction conditions for C-H activation were adapted from literature.[51, 63]

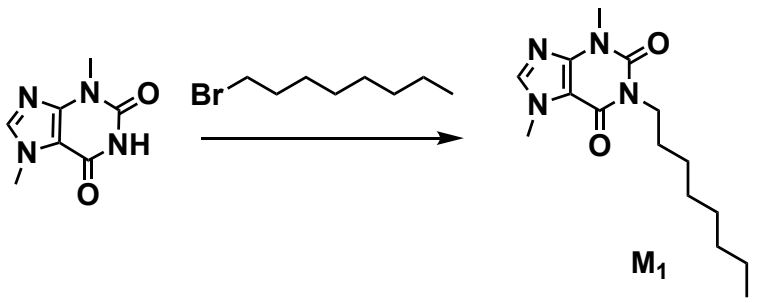

Synthesis of 3,7-dihydro-3,7-dimethyl-1-octyl-1H-purine-2,6-dione (**M1**): 21 g (100 mmol) grinded tripotassium phosphate (K_3PO_4), 9 g (50 mmol) white solid theobromine and 9.65 g (50 mmol) 1-bromooctane were measured and added into flask with 150 ml DMF, which was vacuumed and refilled with nitrogen. The reactants were then heated and refluxed at 140 °C overnight. The reaction mixture was extracted with ethyl acetate (EtOAc) and washed with saturated NH_4Cl solution, dried over anhydrous $MgSO_4$, and concentrated under vacuum to obtain red orange liquid. The liquid was purified by column chromatography (silica gel, DCM/methanol = 12/1) to get 6 g white solid **M1** (yield: 41 %).

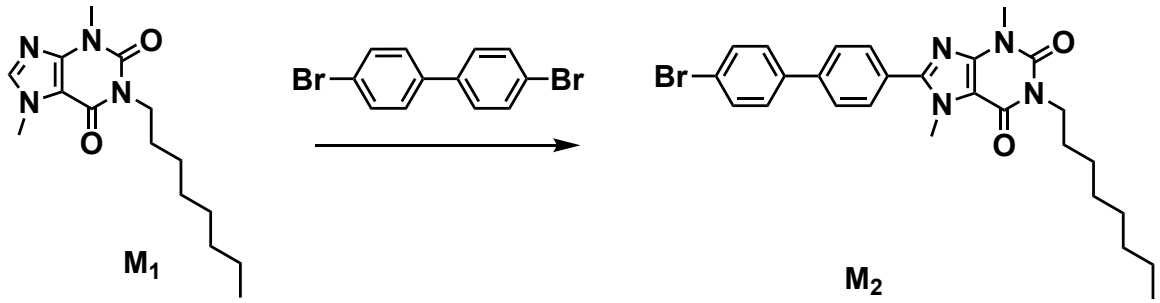

Synthesis of 3,7-dihydro-3,7-dimethyl-8-(4'-bromo[1,1'-biphenyl]-4-yl)-1-octyl-1H-purine-2,6-dione (**M2**): 2.92 g (10 mmol) **M1**, 0.23 g (0.25 mmol) $Pd_2(dba)_3$, 0.35 g (1 mmol) tris(2-methoxyphenyl)phosphine, 6.5 g (20 mmol) Cs_2CO_3, 0.5 g (5 mmol) pivalic acid and 9.36 g (30 mmol) 4,4′-dibromobiphenyl were scaled and added into flask with 100 ml anhydrous toluene, which was vacuumed and refilled with nitrogen. The reaction took place under 110 °C overnight. The reaction mixture was extracted with ethyl acetate and washed with brine, dried over anhydrous

$MgSO_4$, and concentrated under vacuum to obtain yellow solid. The solid dissolved in DCM was purified by column chromatography (silica gel, DCM/EtOAc = 20/1), and recrystallized in methanol to get 2.5 g yellow solid **M2** (yield: 48 %). ^{1}H NMR (500 MHz, $CDCl_3$): 7.82 – 7.72 (d, 2H), 7.74 – 7.66 (d, 2H), 7.63 – 7.57 (d, 2H), 7.52 – 7.44 (d, 2H), 4.10 (s, 3H), 4.09 – 3.99 (m, 2H), 3.63 (s, 3H), 1.72 – 1.63 (m, 2H), 1.43 – 1.20 (m, 10H), 0.90 – 0.80 (t, 3H).

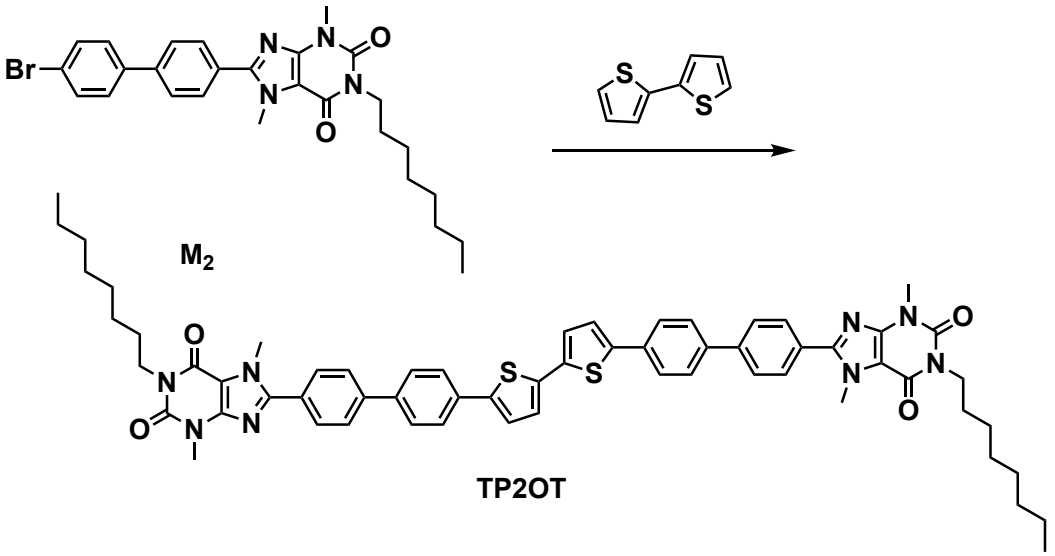

Synthesis of **TP2OT**: 1.286 g (4.4 mmol) **M2**, 46 mg (0.05 mmol) $Pd_2(dba)_3$, 70.5 mg (0.2 mmol) tris(2-methoxyphenyl)phosphine, 1.305 g (4 mmol) Cs_2CO_3, 0.1 g (1 mmol) pivalic acid and 0.333 g (2 mmol) 2,2′-bithiophene were scaled and added into flask with 50 ml anhydrous toluene, which was vacuumed and refilled with nitrogen. The reaction took place under 110 °C overnight. The reaction residue was mixed with silica gel and concentrated under vacuum to obtain yellow powder. The powder dissolved in DCM was purified by column chromatography (silica gel, DCM/methanol = 25/1), and recrystallized in methanol to get 0.23 g yellow solid **TP2OT** (yield: 19 %). ^{1}H NMR (500 MHz, $CDCl_3$): 7.79 (s, 8H), 7.73 (d, 4H), 7.68 (d, 4H), 7.33 (d, 2H), 7.24 (d, 2H), 4.13 (s, 6H), 4.04 (t, 4H), 3.65 (s, 6H), 1.68 (m, 4H), 1.37 – 1.24 (m, 20H), 0.91 – 0.85 (t, 6H).

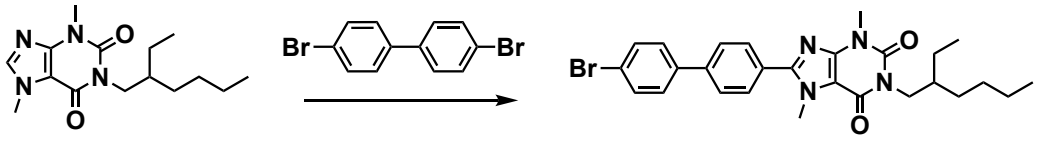

M_1 M_2

Synthesis of 3,7-dihydro-3,7-dimethyl-8-(4'-bromo[1,1'-biphenyl]-4-yl)-1-(2-ethylhexyl)-1H-purine-2,6-dione (**M2**): 2.92 g (10 mmol) **M1**, 0.23 g (0.25 mmol) $Pd_2(dba)_3$, 0.35 g (1 mmol) tris(2-methoxyphenyl)phosphine, 6.5 g (20 mmol) Cs_2CO_3, 0.5 g (5 mmol) pivalic acid and 9.36 g (30 mmol) 4,4′-dibromobiphenyl were scaled and added into flask with 100 ml anhydrous toluene, which was vacuumed and refilled with nitrogen. The reaction took place under 110 °C overnight. The reaction mixture was extracted with ethyl acetate and washed with brine, dried over anhydrous $MgSO_4$, and concentrated under vacuum to obtain yellow solid. The solid dissolved in DCM was purified by column chromatography (silica gel, DCM/EtOAc = 20/1), and recrystallized in methanol to get 1.42 g yellow solid **M2** (yield: 27 %). ^{1}H NMR (500 MHz, $CDCl_3$): 7.83 – 7.72 (d, 2H), 7.72 – 7.65 (d, 2H), 7.64 – 7.55 (d, 2H), 7.53 – 7.45 (d, 2H), 4.10 (s, 3H), 3.96 (m, 2H), 3.63 (s, 3H), 1.89 (m, 1H), 1.42 – 1.22 (m, 8H), 0.91 (m, 6H).

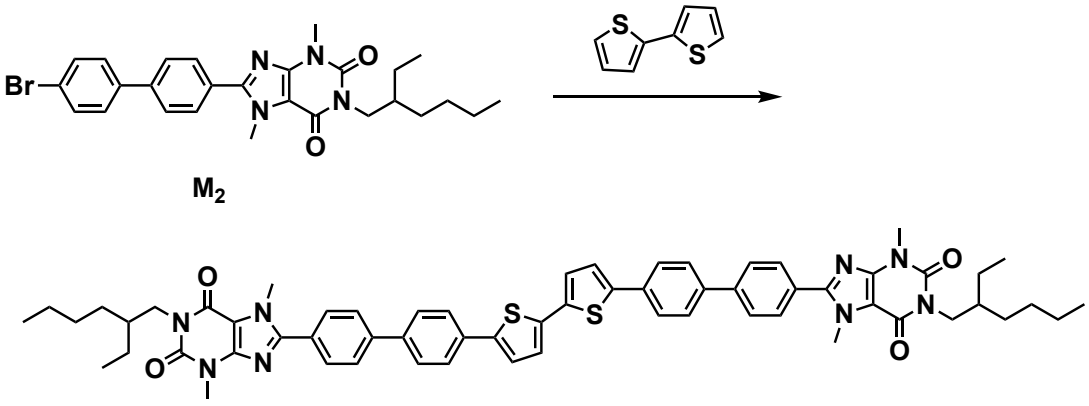

M_2

TP2EHT

Synthesis of **TP2EHT**: 1.286 g (4.4 mmol) **M2**, 46 mg (0.05 mmol) $Pd_2(dba)_3$, 70.5 mg (0.2 mmol) tris(2-methoxyphenyl)phosphine, 1.305 g (4 mmol) Cs_2CO_3, 0.1 g (1 mmol) pivalic acid and 0.333 g (2 mmol) 2,2′-bithiophene were scaled and added into flask with 50 ml anhydrous

toluene, which was vacuumed and refilled with nitrogen. The reaction took place under 110 °C overnight. The reaction residue was mixed with silica gel and concentrated under vacuum to obtain yellow powder. The powder dissolved in $CHCl_3$ was purified by column chromatography (silica gel, $CHCl_3$/methanol = 100/1), and recrystallized in methanol to get 1.04 g orange solid **TP2EHT** (yield: 88 %). ^{1}H NMR (500 MHz, $CDCl_3$): 7.83 – 7.74 (m, 8H), 7.73 (d, 4H), 7.69 (d, 4H), 7.34 (d, 2H), 7.24 (d, 2H), 4.13 (s, 6H), 3.98 (m, 4H), 3.65 (s, 6H), 1.94 – 1.88 (m, 2H), 1.39 - 1.27 (m, 16H), 0.92 (m, 12H).

5.3 OFET Device Fabrication and Characterization

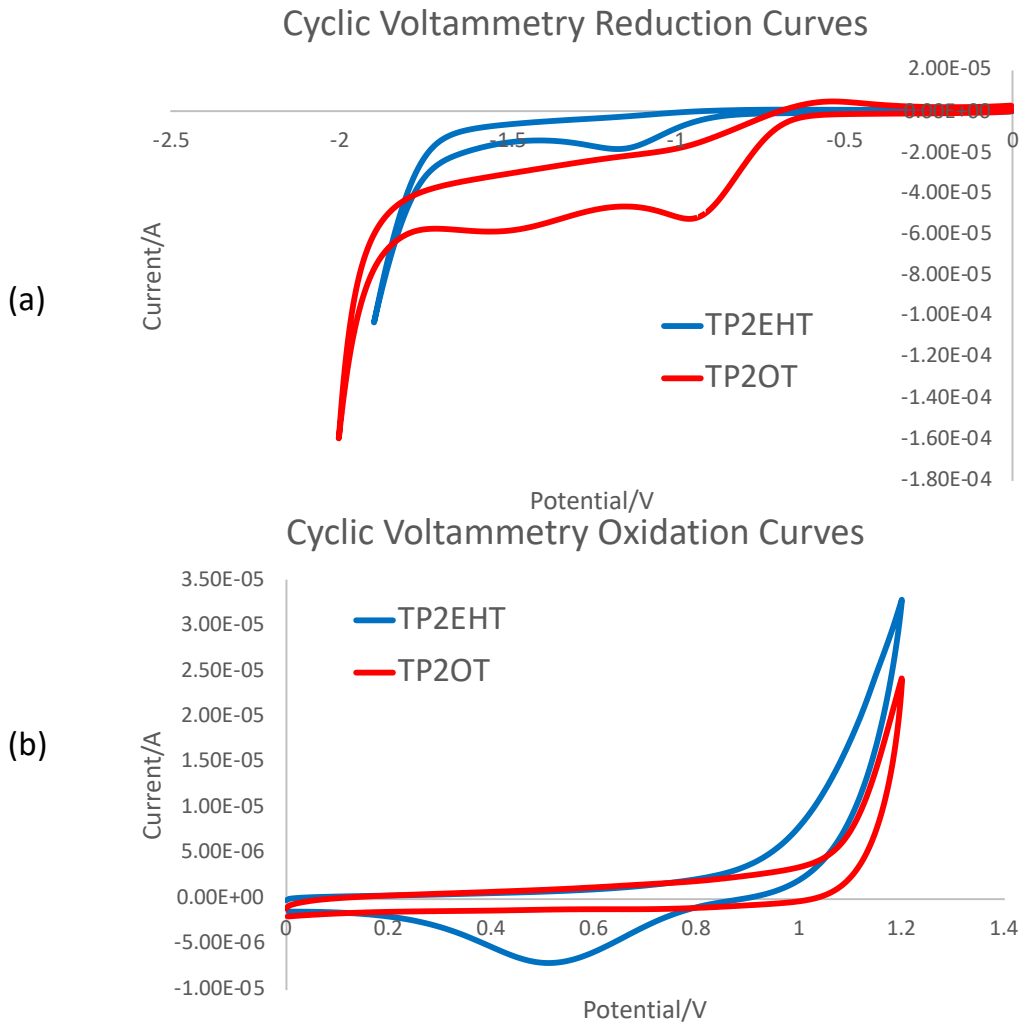

Figure 5.1. Cyclic Voltammetry Curves, (a) Reduction Curves, (b) Oxidation Curves

We chose bottom gate top contact structure for organic field effect transistor, and it was fabricated on p-doped silicon <100> substrate with thermally grown 500 nm silicon oxide as dielectric layer from Montco Silicon Technologies Inc. The substrate was cleaned by ultrasonication in deionized water, acetone, isopropyl alcohol for 15 min respectively, and it was further cleaned by plasma for another 15 min afterwards. Next, self-assembled monolayer (SAM) was deposited onto the surface of substrate by spin coating (3000 rpm for 60s). Semiconductor films were also spin coated from

chloroform solution (1 mg/ml for **TP2OT**, 5 mg/ml for **TP2EHT**) in 2500 rpm for 60s. At last, silver granules in Mo boat were heated under high vacuum (< 10^{-7} torr) to thermally evaporate onto the surface of semiconductor layer *via* shadow mask, acting as source and drain electrodes (W = 1000 μm, L = 50 μm), and indium was inserted into the device functioning as gate electrode.

CV characterization results are shown in Figure 5.1.

BIBLIOGRAPHY

[1] B. Matas, "Semiconductor Shipments Forecast to Exceed 1 Trillion Devices in 2018," *Research Bulletin, Insights, IC,* 2018.

[2] X. Hiao, *Introduction to semiconductor manufacturing technology*. Prentice Hall, 2000.

[3] M. Pope, P. Magnante, and H. P. Kallmann, "ELECTROLUMINESCENCE IN ORGANIC CRYSTALS," *Journal of Chemical Physics,* vol. 38, no. 8, pp. 2042-&, 1963 1963, doi: 10.1063/1.1733929.

[4] W. Helfrich and Schneide.Wg, "RECOMBINATION RADIATION IN ANTHRACENE CRYSTALS," *Physical Review Letters,* vol. 14, no. 7, pp. 229-&, 1965 1965, doi: 10.1103/PhysRevLett.14.229.

[5] W. Helfrich and W. G. Schneider, "TRANSIENTS OF VOLUME-CONTROLLED CURRENT AND OF RECOMBINATION RADIATION IN ANTHRACENE," *Journal of Chemical Physics,* vol. 44, no. 8, pp. 2902-+, 1966 1966, doi: 10.1063/1.1727152.

[6] W. Brütting, "Organic semiconductors," *Semiconductors,* vol. 6, no. 1, p. 11, 2005.

[7] C. K. Chiang *et al.*, "ELECTRICAL-CONDUCTIVITY IN DOPED POLYACETYLENE," *Physical Review Letters,* vol. 39, no. 17, pp. 1098-1101, 1977 1977, doi: 10.1103/PhysRevLett.39.1098.

[8] C. W. Tang, "2-LAYER ORGANIC PHOTOVOLTAIC CELL," *Applied Physics Letters,* vol. 48, no. 2, pp. 183-185, Jan 13 1986, doi: 10.1063/1.96937.

[9] A. Tsumura, H. Koezuka, and T. Ando, "POLYTHIOPHENE FIELD-EFFECT TRANSISTOR - ITS CHARACTERISTICS AND OPERATION MECHANISM," *Synthetic Metals,* vol. 25, no. 1, pp. 11-23, Jul 1988, doi: 10.1016/0379-6779(88)90318-9.

[10] M. Pope and C. E. Swenberg, *Electronic processes in organic crystals and polymers*, 2nd ed. (Monographs on the physics and chemistry of materials, no. #56). New York: Oxford University Press, 1999, pp. xxix, 1328 pages.

[11] L. Li and H. Kosina, "Charge Transport in Organic Semiconductor Devices," in *Organic Electronics*, T. Grasser, G. Meller, and L. Li Eds. Berlin, Heidelberg: Springer Berlin Heidelberg, 2010, pp. 301-323.

[12] A. J. Heeger, "Semiconducting polymers: the Third Generation," *Chemical Society Reviews,* vol. 39, no. 7, pp. 2354-2371, 2010 2010, doi: 10.1039/b914956m.

[13] B. S. Ong, Y. Wu, Y. Li, P. Liu, and H. Pan, "Thiophene polymer semiconductors for organic thin-film transistors," *Chemistry-a European Journal,* vol. 14, no. 16, pp. 4766-4778, 2008 2008, doi: 10.1002/chem.200701717.

[14] G. Li, R. Zhu, and Y. Yang, "Polymer solar cells," (in English), *Nature Photonics,* Review vol. 6, no. 3, pp. 153-161, Mar 2012, doi: 10.1038/nphoton.2012.11.

[15] J. T. E. Quinn, J. Zhu, X. Li, J. Wang, and Y. Li, "Recent progress in the development of n-type organic semiconductors for organic field effect transistors," *Journal of Materials Chemistry C,* vol. 5, no. 34, pp. 8654-8681, Sep 14 2017, doi: 10.1039/c7tc01680h.

[16] J. E. Anthony, A. Facchetti, M. Heeney, S. R. Marder, and X. Zhan, "n-Type Organic Semiconductors in Organic Electronics," *Advanced Materials,* vol. 22, no. 34, pp. 3876-3892, Sep 8 2010, doi: 10.1002/adma.200903628.

[17] X. Guo and M. D. Watson, "Conjugated Polymers from Naphthalene Bisimide," *Organic Letters,* vol. 10, no. 23, pp. 5333-5336, Dec 4 2008, doi: 10.1021/ol801918y.

[18] L. E. Polander *et al.*, "Benzothiadiazole-Dithienopyrrole Donor-Acceptor-Donor and Acceptor-Donor-Acceptor Triads: Synthesis and Optical, Electrochemical, and Charge-Transport Properties," *Journal of Physical Chemistry C,* vol. 115, no. 46, pp. 23149-23163, Nov 24 2011, doi: 10.1021/jp208643k.

[19] A. Facchetti, "Semiconductors for organic transistors," *Materials Today,* vol. 10, no. 3, pp. 28-37, 2007.

[20] Y. Y. Lin, D. J. Gundlach, S. F. Nelson, and T. N. Jackson, "Stacked pentacene layer organic thin-film transistors with improved characteristics," *Ieee Electron Device Letters,* vol. 18, no. 12, pp. 606-608, Dec 1997, doi: 10.1109/55.644085.

[21] G. Horowitz, "Field-effect transistors based on short organic molecules," *Journal of Materials Chemistry,* vol. 9, no. 9, pp. 2021-2026, Sep 1999, doi: 10.1039/a902242b.

[22] J. G. Laquindanum, H. E. Katz, A. J. Lovinger, and A. Dodabalapur, "Benzodithiophene rings as semiconductor building blocks," *Advanced Materials,* vol. 9, no. 1, pp. 36-&, Jan 1997, doi: 10.1002/adma.19970090106.

[23] X. C. Li *et al.*, "A highly pi-stacked organic semiconductor for thin film transistors based on fused thiophenes," *Journal of the American Chemical Society,* vol. 120, no. 9, pp. 2206-2207, Mar 11 1998, doi: 10.1021/ja9735968.

[24] J. G. Laquindanum, H. E. Katz, A. Dodabalapur, and A. J. Lovinger, "n-channel organic transistor materials based on naphthalene frameworks," *Journal of the American Chemical Society,* vol. 118, no. 45, pp. 11331-11332, Nov 13 1996, doi: 10.1021/ja962461j.

[25] A. R. Brown, D. M. Deleeuw, E. J. Lous, and E. E. Havinga, "ORGANIC N-TYPE FIELD-EFFECT TRANSISTOR," *Synthetic Metals,* vol. 66, no. 3, pp. 257-261, Oct 1994, doi: 10.1016/0379-6779(94)90075-2.

[26] L. Zhang *et al.*, "Conjugated Polymers Based on Thiazole Flanked Naphthalene Diimide for Unipolar n-Type Organic Field-Effect Transistors," *Chemistry of Materials,* vol. 30, no. 22, pp. 8343-8351, Nov 27 2018, doi: 10.1021/acs.chemmater.8b03902.

[27] H. Antoniadis, B. R. Hsieh, M. A. Abkowitz, S. A. Jenekhe, and M. Stolka, "PHOTOVOLTAIC AND PHOTOCONDUCTIVE PROPERTIES OF ALUMINUM POLY(P-PHENYLENE VINYLENE) INTERFACES," *Synthetic Metals,* vol. 62, no. 3, pp. 265-271, Feb 1994, doi: 10.1016/0379-6779(94)90215-1.

[28] W. Riess, S. Karg, V. Dyakonov, M. Meier, and M. Schwoerer, "ELECTROLUMINESCENCE AND PHOTOVOLTAIC EFFECT IN PPV SCHOTTKY DIODES," *Journal of Luminescence,* vol. 60-1, pp. 906-911, Apr 1994.

[29] G. Yu, J. Gao, J. C. Hummelen, F. Wudl, and A. J. Heeger, "POLYMER PHOTOVOLTAIC CELLS - ENHANCED EFFICIENCIES VIA A NETWORK OF INTERNAL DONOR-ACCEPTOR HETEROJUNCTIONS," *Science,* vol. 270, no. 5243, pp. 1789-1791, Dec 1995, doi: 10.1126/science.270.5243.1789.

[30] J. J. M. Halls *et al.*, "EFFICIENT PHOTODIODES FROM INTERPENETRATING POLYMER NETWORKS," *Nature,* vol. 376, no. 6540, pp. 498-500, Aug 1995, doi: 10.1038/376498a0.

[31] L. Meng *et al.*, "Organic and solution-processed tandem solar cells with 17.3% efficiency," *Science,* vol. 361, no. 6407, pp. 1094-+, Sep 14 2018, doi: 10.1126/science.aat2612.

[32] Y. Huang and C. K. Luscombe, "Towards Green Synthesis and Processing of Organic Solar Cells," *Chemical record (New York, N.Y.),* 2019-Jan-15 2019, doi: 10.1002/tcr.201800145.

[33] C. Sekine, Y. Tsubata, T. Yamada, M. Kitano, and S. Doi, "Recent progress of high performance polymer OLED and OPV materials for organic printed electronics," *Science and Technology of Advanced Materials,* vol. 15, no. 3, Jun 2014, Art no. 034203, doi: 10.1088/1468-6996/15/3/034203.

[34] C. H. Oh, H. J. Shin, W. J. Nam, B. C. Ahn, S. Y. Cha, and S. D. Yeo, "21.1: Invited paper: Technological progress and commercialization of OLED TV," in *SID Symposium Digest of Technical Papers*, 2013, vol. 44, no. 1: Wiley Online Library, pp. 239-242.

[35] F. Ebisawa, T. Kurokawa, and S. Nara, "ELECTRICAL-PROPERTIES OF POLYACETYLENE POLYSILOXANE INTERFACE," *Journal of Applied Physics,* vol. 54, no. 6, pp. 3255-3259, 1983 1983, doi: 10.1063/1.332488.

[36] A. Tsumura, H. Koezuka, and T. Ando, "MACROMOLECULAR ELECTRONIC DEVICE - FIELD-EFFECT TRANSISTOR WITH A POLYTHIOPHENE THIN-FILM," *Applied Physics Letters,* vol. 49, no. 18, pp. 1210-1212, Nov 3 1986, doi: 10.1063/1.97417.

[37] H. Dong, X. Fu, J. Liu, Z. Wang, and W. Hu, "25th Anniversary Article: Key Points for High-Mobility Organic Field-Effect Transistors," *Advanced Materials,* vol. 25, no. 43, pp. 6158-6182, Nov 20 2013, doi: 10.1002/adma.201302514.

[38] O. D. Jurchescu, M. Popinciuc, B. J. van Wees, and T. T. M. Palstra, "Interface-controlled, high-mobility organic transistors," *Advanced Materials,* vol. 19, no. 5, pp. 688-+, Mar 5 2007, doi: 10.1002/adma.200600929.

[39] H. Li *et al.*, "High-Mobility Field-Effect Transistors from Large-Area Solution-Grown Aligned C-60 Single Crystals," *Journal of the American Chemical Society,* vol. 134, no. 5, pp. 2760-2765, Feb 8 2012, doi: 10.1021/ja210430b.

[40] I. Kymissis, *Organic field effect transistors: theory, fabrication and characterization*. Springer Science & Business Media, 2008.

[41] Y. Xu, C. Liu, D. Khim, and Y.-Y. Noh, "Development of high-performance printed organic field-effect transistors and integrated circuits," *Physical Chemistry Chemical Physics,* vol. 17, no. 40, pp. 26553-26574, 2015 2015, doi: 10.1039/c4cp02413c.

[42] C.-a. Di, G. Yu, Y. Liu, and D. Zhu, "High-performance organic field-effect transistors: Molecular design, device fabrication, and physical properties," *Journal of Physical Chemistry B,* vol. 111, no. 51, pp. 14083-14096, Dec 27 2007, doi: 10.1021/jp071753b.

[43] L. Leonat, G. Sbarcea, and I. V. Branzoi, "Cyclic voltammetry for energy levels estimation of organic materials," *UPB Sci Bull Ser B,* vol. 75, pp. 111-118, 2013.

[44] A. B. Koren, M. D. Curtis, A. H. Francis, and J. W. Kampf, "Intermolecular interactions in pi-stacked conjugated molecules. Synthesis, structure, and spectral characterization of alkyl bithiazole oligomers," *Journal of the American Chemical Society,* vol. 125, no. 17, pp. 5040-5050, Apr 30 2003, doi: 10.1021/ja029216m.

[45] E. Tapavicza, F. Furche, and D. Sundholm, "Importance of Vibronic Effects in the UV-Vis Spectrum of the 7,7,8,8-Tetracyanoquinodimethane Anion," *Journal of Chemical Theory and Computation,* vol. 12, no. 10, pp. 5058-5066, Oct 2016, doi: 10.1021/acs.jctc.6b00720.

[46] H. L. Gomes, "Organic Field-Effect Transistors," ed: CRC Press: Boca Raton, FL, 2016, pp. 147-197.

[47] J. C. Perkinson, "Organic field-effect transistors," ed, 2007.

[48] J. Chang, Z. Lin, C. Zhang, and Y. Hao, "Organic Field-Effect Transistor: Device Physics, Materials, and Process," in *Different Types of Field-Effect Transistors-Theory and Applications*: IntechOpen, 2017.

[49] Y. Lei, B. Wu, W.-K. E. Chan, F. Zhu, and B. S. Ong, "Engineering gate dielectric surface properties for enhanced polymer field-effect transistor performance," *Journal of Materials Chemistry C,* vol. 3, no. 47, pp. 12267-12272, 2015 2015, doi: 10.1039/c5tc02579f.

[50] J. Veres, S. Ogier, G. Lloyd, and D. de Leeuw, "Gate insulators in organic field-effect transistors," *Chemistry of Materials,* vol. 16, no. 23, pp. 4543-4555, Nov 16 2004, doi: 10.1021/cm049598q.

[51] Y. Segawa, T. Maekawa, and K. Itami, "Synthesis of Extended p-Systems through C-H Activation," *Angewandte Chemie-International Edition,* vol. 54, no. 1, pp. 66-81, Jan 2 2015, doi: 10.1002/anie.201403729.

[52] S. P. Stanforth, "Catalytic cross-coupling reactions in biaryl synthesis," *Tetrahedron,* vol. 54, no. 3-4, pp. 263-303, Jan 15 1998, doi: 10.1016/s0040-4020(97)10233-2.

[53] Y. Yang, J. Lan, and J. You, "Oxidative C-H/C-H Coupling Reactions between Two (Hetero)arenes," *Chemical Reviews,* vol. 117, no. 13, pp. 8787-8863, Jul 12 2017, doi: 10.1021/acs.chemrev.6b00567.

[54] L. McMurray, F. O'Hara, and M. J. Gaunt, "Recent developments in natural product synthesis using metal-catalysed C-H bond functionalisation," *Chemical Society Reviews,* vol. 40, no. 4, pp. 1885-1898, 2011 2011, doi: 10.1039/c1cs15013h.

[55] J. Yamaguchi, A. D. Yamaguchi, and K. Itami, "C-H Bond Functionalization: Emerging Synthetic Tools for Natural Products and Pharmaceuticals," *Angewandte Chemie-International Edition,* vol. 51, no. 36, pp. 8960-9009, 2012 2012, doi: 10.1002/anie.201201666.

[56] K. Okamoto, J. Zhang, J. B. Housekeeper, S. R. Marder, and C. K. Luscombe, "C-H Arylation Reaction: Atom Efficient and Greener Syntheses of pi-Conjugated Small Molecules and Macromolecules for Organic Electronic Materials," *Macromolecules,* vol. 46, no. 20, pp. 8059-8078, Oct 22 2013, doi: 10.1021/ma401190r.

[57] L. Ackermann, R. Vicente, and A. R. Kapdi, "Transition-Metal-Catalyzed Direct Arylation of (Hetero)Arenes by C-H Bond Cleavage," *Angewandte Chemie-International Edition,* vol. 48, no. 52, pp. 9792-9826, 2009 2009, doi: 10.1002/anie.200902996.

[58] G. P. McGlacken and L. M. Bateman, "Recent advances in aryl-aryl bond formation by direct arylation," *Chemical Society Reviews,* vol. 38, no. 8, pp. 2447-2464, 2009 2009, doi: 10.1039/b805701j.

[59] Y. Fujiwara, I. Moritani, S. Danno, R. Asano, and Teranish.S, "AROMATIC SUBSTITUTION OF OLEFINS .6. ARYLATION OF OLEFINS WITH PALLADIUM(II) ACETATE," *Journal of the American Chemical Society,* vol. 91, no. 25, pp. 7166-&, 1969 1969, doi: 10.1021/ja01053a047.

[60] D. Alberico, M. E. Scott, and M. Lautens, "Aryl-aryl bond formation by transition-metal-catalyzed direct arylation," *Chemical Reviews,* vol. 107, no. 1, pp. 174-238, Jan 2007, doi: 10.1021/cr0509760.

[61] J. W. Daly, W. Padgett, M. T. Shamim, P. Buttslamb, and J. Waters, "1,3-DIALKYL-8-(PARA-SULFOPHENYL)XANTHINES - POTENT WATER-SOLUBLE ANTAGONISTS FOR A1-ADENOSINE AND A2-ADENOSINE RECEPTORS," *Journal of Medicinal Chemistry,* vol. 28, no. 4, pp. 487-492, 1985 1985, doi: 10.1021/jm00382a018.

[62] R. V. Kalla *et al.*, "Novel 1,3-disubstituted 8-(1-benzyl-1H-pyrazol-4-yl) xanthines: High affinity and selective A(2B) adenosine receptor antagonists," *Journal of Medicinal Chemistry,* vol. 49, no. 12, pp. 3682-3692, Jun 15 2006, doi: 10.1021/jm051268+.

[63] D. Zhao, W. Wang, S. Lian, F. Yang, J. Lan, and J. You, "Phosphine-Free, Palladium-Catalyzed Arylation of Heterocycles through C-H Bond Activation with Pivalic Acid as a Cocatalyst," *Chemistry-a European Journal,* vol. 15, no. 6, pp. 1337-1340, 2009 2009, doi: 10.1002/chem.200802001.

[64] D. Zhao *et al.*, "Copper-Catalyzed Direct C Arylation of Heterocycles with Aryl Bromides: Discovery of Fluorescent Core Frameworks," *Angewandte Chemie-International Edition,* vol. 48, no. 18, pp. 3296-3300, 2009 2009, doi: 10.1002/anie.200900413.

[65] T. Kono *et al.*, "High-performance and light-emitting n-type organic field-effect transistors based on dithienylbenzothiadiazole and related heterocycles," *Chemistry of Materials,* vol. 19, no. 6, pp. 1218-1220, Mar 20 2007, doi: 10.1021/cm062889+.

[66] J. L. Lakey Beitia, "Tripotassium Phosphate: From Buffers to Organic Synthesis," *Synlett,* no. 1, pp. 139-140, Jan 2011, doi: 10.1055/s-0030-1259092.

[67] F. Wuerthner, T. E. Kaiser, and C. R. Saha-Moeller, "J-Aggregates: From Serendipitous Discovery to Supramolecular Engineering of Functional Dye Materials," *Angewandte Chemie-International Edition,* vol. 50, no. 15, pp. 3376-3410, 2011 2011, doi: 10.1002/anie.201002307.

[68] J.-L. Bredas, "Mind the gap!," *Materials Horizons,* vol. 1, no. 1, pp. 17-19, Jan 2014, doi: 10.1039/c3mh00098b.

[69] J. Rumble, *CRC handbook of chemistry and physics*. CRC press, 2017.

[70] J. F. M. Hardigree *et al.*, "Reducing Leakage Currents in n-Channel Organic Field-Effect Transistors Using Molecular Dipole Mono layers on Nanoscale Oxides," *Acs Applied Materials & Interfaces,* vol. 5, no. 15, pp. 7025-7032, Aug 14 2013, doi: 10.1021/am401278p.

[71] M. Devynck, P. Tardy, G. Wantz, Y. Nicolas, and L. Hirsch, "Organic field-effect transistor with octadecyltrichlorosilane (OTS) self-assembled monolayers on gate oxide: effect of OTS quality," *European Physical Journal-Applied Physics,* vol. 56, no. 3, Dec 2011, Art no. 34106, doi: 10.1051/epjap/2011110138.

[72] C. Huang, H. E. Katz, and J. E. West, "Solution-processed organic field-effect transistors and unipolar inverters using self-assembled interface dipoles on gate dielectrics," *Langmuir,* vol. 23, no. 26, pp. 13223-13231, Dec 18 2007, doi: 10.1021/la702409m.

[73] R. Hamilton *et al.*, "High-Performance Polymer-Small Molecule Blend Organic Transistors," *Advanced Materials,* vol. 21, no. 10-11, pp. 1166-1171, Mar 20 2009, doi: 10.1002/adma.200801725.

[74] A. Campos, S. Riera-Galindo, J. Puigdollers, and M. Mas-Torrent, "Reduction of Charge Traps and Stability Enhancement in Solution-Processed Organic Field-Effect Transistors Based on a Blended n-Type Semiconductor," *Acs Applied Materials & Interfaces,* vol. 10, no. 18, pp. 15952-15961, May 9 2018, doi: 10.1021/acsami.8b02851.

[75] M. Mas-Torrent, P. Hadley, S. T. Bromley, N. Crivillers, J. Veciana, and C. Rovira, "Single-crystal organic field-effect transistors based on dibenzo-tetrathiafulvalene," *Applied Physics Letters,* vol. 86, no. 1, Jan 3 2005, Art no. 012110, doi: 10.1063/1.1848179.